
A Geometric View for Understanding Concept Learning and Neuron Interpretation in Sparse Autoencoders

Chenhao Zhang^{*1} Chris Lin^{*1} Su-In Lee¹

Abstract

We propose a unified mathematical framework for a geometric understanding of concept learning and neuron interpretation in sparse autoencoders (SAEs). While SAEs improve interpretability of neural networks by learning sparse feature representations, a principled definition of "concept" and "learning" remains unclear. We formalize concepts as sets of data points and cast concept learning as a set-alignment problem between human-defined and model-induced concepts. This formulation distinguishes three increasingly strong notions of learning—detection, separation, and approximation—and yields geometric conditions, error bounds, and capacity constraints for when concepts can be represented by individual neurons or multi-neuron units. It also provides a set-theoretic account for common SAE phenomena, including feature splitting, feature absorption, feature families, and hierarchical concepts. Finally, we connect concept learning and neuron interpretation through formal concept analysis, showing that the two directions need not agree and that their many-to-many structure can be organized by concept lattices. Experiments on synthetic data with ReLU and Top- K SAEs illustrate the theory and reveal the effects of SAE size and sparsity on concept learning.

1. Introduction

Large models based on neural networks achieve remarkable performance across many tasks, yet their internal mechanisms remain largely opaque (Elhage et al., 2021; Olah, 2022). This lack of interpretability limits scientific understanding (DeGrave et al., 2021; Simon & Zou, 2025), safety auditing (Anwar et al., 2024a;b), and reliable deployment. Mechanistic interpretability (Elhage et al., 2021;

Olah, 2022) aims to understand the internal computations of models by analyzing how information is represented and used within model activations.

A major challenge is that neurons in neural networks are mostly polysemantic (Templeton, 2024). A single neuron may encode multiple unrelated concepts, while a single concept may be distributed across many neurons. This phenomenon, known as polysemanticity or superposition (Templeton, 2024; Elhage et al., 2022; O’Neill et al., 2024), makes neuron-level interpretation difficult. Sparse autoencoders (SAEs) (Ng et al., 2011) address this by learning overcomplete sparse representations of activations, producing neurons that are often more interpretable and monosemantic (Cunningham et al., 2023).

SAEs are commonly motivated by the linear representation hypothesis (Park et al., 2023), which posits that semantically meaningful concepts correspond to directions in the activation space and are approximately linearly combined. However, vector directions alone do not define human-interpretable concepts in practice. Instead, interpretation needs to be contextualized with respect to input data. Specifically, data examples that highly activate a neuron are identified, and their shared patterns are summarized to describe the neuron (Bills et al., 2023). Thus, SAE interpretation also fundamentally relies on relationships between internal neurons and sets of data examples.

This perspective becomes particularly important in light of empirical SAE phenomena. SAE neurons can resolve polysemanticity (Cunningham et al., 2023; O’Neill et al., 2024); larger SAEs may split coarse neurons into finer semantic components (O’Neill et al., 2024; Bricken et al., 2023); feature absorption may occur when one neuron captures examples expected to belong to another (Chanin et al., 2024); and groups of neurons may co-activate as a feature family (Bricken et al., 2023). These observations suggest that SAE neurons are not isolated vectors with fixed meanings, but part of a structured relationship defined through input data, activations, and human-interpretable abstractions. Despite extensive empirical study, we still lack a unified framework that explains when these phenomena arise, how they relate to activation geometry (Costa et al., 2025; Fel et al., 2025).

¹Paul G. Allen School of Computer Science & Engineering, University of Washington, Seattle, USA. Correspondence to: Su-In Lee <suinlee@cs.washington.edu>.

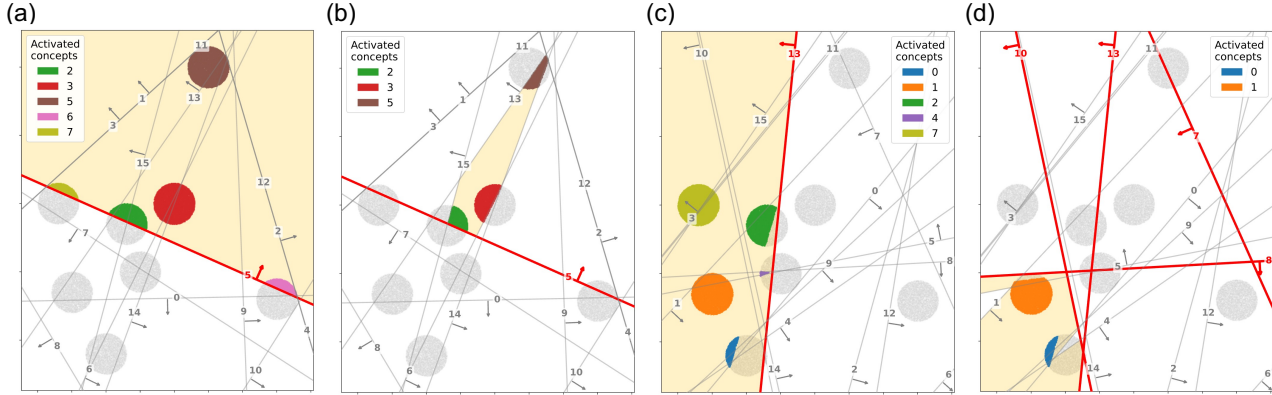


Figure 1. Examples of single neuron total activation (SNTA) and total neuron single activation (TNSA) of ReLU SAE (expansion factor=8 and L1 regularization=0.5) and Topk-K SAE (expansion factor=8 and K=4). (a) SNTA of ReLU SAE, (b) TNSA of ReLU SAE; note that the SNTA of ReLU SAE is simply a half space and TNSA is a hyperplane arrangement region (Stanley et al., 2007). (c) SNTA of Top-K SAE, (d) TNSA of Top-K SAE; note that the SNTA of Top-K SAE is a subset of a half space and its TNSA is a subset of a hyperplane arrangement region. The shaded area in (d) is the intersection of positively pre-activated (i.e., $z > 0$) hyperplanes and negatively pre-activated (i.e., $z < 0$) hyperplanes.

At the root of this difficulty lies a more fundamental ambiguity: neither “concept” nor “learning” is formally defined in most discussions of concept learning and neuron interpretation (Ayonrinde & Jaburi, 2025). This ambiguity echoes a long-standing philosophical debate. A Platonic or realist view treats concepts as abstract entities independent of their instances, whereas a nominalist or data-grounded view treats concepts as abstractions constructed from collections of examples. Machine learning is closer to the latter. That is, models are trained on empirical data, and interpretations are validated through examples associated with internal neurons. From this data-grounded perspective, a neuron should not be assumed to be a primitive object such as a single vector, but rather interpreted as a set of data points associated with the neuron.

The data-grounded view also clarifies what it means for a model to learn a concept. Human concepts such as “animal” or “food” correspond to coherent sets of examples that humans can group and describe. A neuron in a model learns a human concept only when the examples associated with the neuron align with a human-understandable set. Conversely, when a neuron activates on heterogeneous examples lacking a coherent abstraction, we regard it as polysemantic or uninterpretable. In this work, we propose a novel framework for understanding concept learning and neuron interpretation.

We formulate both concept learning and neuron interpretation as a set-alignment problem between human concepts and model-induced concepts, where concept corresponds to a set and learning corresponds to alignment. And it is the implicit bias and underlying assumptions in both data and model that makes concept learning and neuron interpretation possible.

Under this view, neuron interpretation corresponds to how to characterize the set selected by a neuron or SAE neuron, while concept learning corresponds to whether the learned set aligns with a target human concept.

Therefore, in our proposed mathematical framework, we represent concepts as sets and study their alignment through geometric and set-theoretic structures. This framework distinguishes different modes of concept learning, derives conditions under which they arise, and explains empirical SAE phenomena such as feature splitting, feature absorption, and feature families. We further connect concept learning and neuron interpretation through formal concept lattices, providing a formulation for representing hierarchical concept structure.

To summarize, our contributions are as follows:

1. We propose a unified geometric and set-theoretic framework for concept learning, human concept alignment, and SAE interpretation, formulating concept learning as set alignment between human-understandable and model-induced concepts.
2. We distinguish three modes of concept learning—concept detection, concept separation, and concept formation—and derive sufficient and necessary conditions, along with scaling laws governing when each mode is achievable.
3. We show that concept learning and neuron interpretation are related but distinct, and connect them through formal concept lattices that characterize hierarchical structure and neuron semantics.

2. Related Work

Mechanistic Interpretability and Sparse Autoencoders. Mechanistic interpretability studies the internal computa-

tions of large models (Elhage et al., 2021; Olah, 2022; Olsson et al., 2022). A key challenge is superposition, where multiple concepts are represented in overlapping neural directions (Elhage et al., 2022). Sparse autoencoders (SAEs), closely related to dictionary learning (Olshausen & Field, 1997), learn overcomplete sparse features that reconstruct model activations (Ng et al., 2011). Recent work shows that SAEs can disentangle superposed representations and recover more monosemantic, human-interpretable features (Cunningham et al., 2023; O’Neill et al., 2024; Templeton, 2024). More recently, Bhalla et al. (2026) find that concepts lie on a low-dimensional shape and that SAEs can globally and locally capture the concept manifold. Our work is a generalization of Park et al. (2023) and Bhalla et al. (2026), because we study the general case of concepts in a set-theoretic framework where concepts can be arbitrary measurable sets.

SAE Architectures and Phenomena. A growing literature studies empirical phenomena in SAE features, including polysemanticity and monosemanticity (Elhage et al., 2022), feature splitting and feature families (Cunningham et al., 2023; Bricken et al., 2023), and feature absorption (Chanin et al., 2024). Several SAE variants aim to improve sparsity, feature quality, or structure, including Gated SAEs (Rajamanoharan et al., 2024a), JumpReLU SAEs (Rajamanoharan et al., 2024b), Top- K SAEs (Gao et al., 2024), matching-pursuit SAEs (Costa et al., 2025), ensemble SAEs (Gadgil et al., 2025), SPaDE (Hindupur et al., 2025), and hierarchical SAEs (Leask et al., 2025; Muchane et al., 2025). In particular, hierarchical and matching-pursuit SAEs seek to capture hierarchical or conditional relationships among concepts. However, recent work also raises concerns: SAEs may find seemingly interpretable features in randomly initialized transformers (Heap et al., 2025), and very large SAEs can learn pathological concepts (Michaud et al., 2025).

Concept Learning and Neuron Interpretation. The linear representation hypothesis posits that concepts are represented as directions in activation space and combined approximately linearly (Park et al., 2023). Since such directions are not directly interpretable, neuron interpretation methods often explain a neuron or feature using its most activating examples. For example, Bills et al. (2023) use an LLM to infer concepts from highly activating and random samples, with related work studying black-box neuron interpretation (Singh et al., 2023). Complementary concept-based methods instead start from data or predefined concepts and search for corresponding neurons or directions (Gurnee et al., 2023; Koh et al., 2020). Evaluation is crucial for such associations, with Oikarinen et al. (2025) summarizing metrics and proposing criteria for testing interpretation faithfulness. Recent work further suggests that concepts may be represented by richer geometric structures rather

than single linear directions (Fel et al., 2025; Shafran et al., 2026; Sarfati et al., 2026; Costa et al., 2025; Hindupur et al., 2025).

Network Capacity and Hyperplane Arrangements. Neural network expressivity is often studied through the regions induced by activation patterns, with the number of regions serving as a measure of capacity (Montúfar et al., 2014; Pascanu et al., 2013). This view connects naturally to hyperplane arrangements, where neurons define hyperplanes that partition representation space (Stanley et al., 2007). Closely related to sparse selection mechanisms, Su et al. (2026) analyze the capacity of Top- K mixture-of-expert networks by casting expert selection as a hyperplane arrangement problem. This geometric perspective is relevant for understanding the capacity of Top- K SAEs and related sparse architectures.

3. Preliminaries

We first review sparse autoencoders (SAEs), focusing on ReLU SAE (Cunningham et al., 2023) and Top- K SAE (Gao et al., 2024). Let $x \in \mathbb{R}^n$ be an activation vector from a large model. An SAE maps x to a higher-dimensional sparse activation vector $a \in \mathbb{R}^d$, where $d \gg n$, and then reconstructs x from a :

$$\begin{aligned} z &= Enc(x) = W_{enc}(x - b_{pre}) + b_{enc}, \\ a &= Act(z), \\ \hat{x} &= Dec(a) = W_{dec}a + b_{dec}. \end{aligned}$$

Here Act is the SAE activation function, a_i is the activation of the i -th SAE neuron, and \hat{x} is the reconstruction of x . For ReLU SAE, Act is the ReLU function, and the objective is usually written as $\mathcal{L}_{ReLU} = \|x - \hat{x}\|_2^2 + \lambda \|a\|_1$. For Top- K SAE, Act keeps only the k largest coordinates of the pre-activation vector and sets the rest to zero, imposing a hard sparsity constraint, and the objective is $\mathcal{L}_{topk} = \|x - \hat{x}\|_2^2$.

Throughout the paper, with a slight abuse of notation, we denote W, b for W_{enc}, b_{enc} , respectively, and $a_i(x) = Act(\langle w_i, x \rangle + b_i)$ for the activation of SAE neuron i .

4. Main Framework

4.1. Notations and Definitions

Concepts. Let $X \subseteq \mathbb{R}^n$ denote the SAE input space, i.e., the activation space of the original model. Although concepts and interpretations are usually described in the raw data space, (Nikolaou et al., 2025) shows that the LLM imposes an invertible map between the raw data space and its internal activation space. Thus, here we consider working in the internal space as equivalent to working in the raw data space. We equip X with the Borel algebra $\mathcal{B}(X)$. A human-understandable concept is a measurable set $C \in \mathcal{B}(X)$, and

the human concept set is $\mathcal{C} \subseteq \mathcal{B}(X)$. We use μ for the data-supported measure used in concept detection and concept separation, and ν for a measure on the ambient space used in concept approximation. Details are discussed in Section 4.3. Intuitively, μ evaluates only observed data, whereas ν also evaluates blank or novel regions outside the observed data support.

SAE Neurons. For a neuron i , define the threshold set and its two sides by

$$\begin{aligned} H_i^+ &= \{x \in X : z_i(x) > \tau_i\}, \\ H_i^- &= \{x \in X : z_i(x) \leq \tau_i\}, \end{aligned}$$

where τ_i is a threshold. For ReLU SAE, we usually take $\tau_i = 0$. The positive side H_i^+ is called the *activation region* of neuron i under ReLU gating.

SAE Activations. An *activation pattern* s assigns a sign $\sigma_{s;i} \in \{+, -\}$ to every neuron. Its corresponding *total neuron single activation* (TNSA) region is

$$R_s = \bigcap_{i \in [d]} H_i^{\sigma_{s;i}}. \quad (1)$$

The collection of all activation patterns, or equivalently the corresponding TNSA regions, is denoted by \mathcal{A} . The sparsity of a pattern is $|\{i : \sigma_{s;i} = +\}|$.

The *single-neuron total activation* (SNTA), or simply the activation region of neuron i , is

$$N_i = \bigcup_{s \in \mathcal{A}: \sigma_{s;i} = +} R_s. \quad (2)$$

For ReLU SAE, $N_i = H_i^+$. For Top-K SAE, however, N_i is generally only a subset of H_i^+ , because a neuron with a positive score may still fail to enter the top- k set. An example is shown in Figure 1. This distinction is important and discussed in Section 4.2.

For a set of neurons $M \subseteq [d]$, define the *multi-neuron activation* as

$$\theta_M = \bigcap_{j \in M} N_j. \quad (3)$$

The collection of model-learned concepts is denoted by

$$\Theta = \{\theta_M : M \subseteq [d]\}. \quad (4)$$

We argue that concept learning and neuron interpretation should use θ_M rather than only N_i or R_s : N_i can be too large and may cover many unrelated regions, leading to polysemanticity, while R_s can be too small, making model-learned concepts fragile. By aggregating selected neurons, θ_M provides a useful granularity for concept learning and neuron interpretation. Examples are shown in Figure 1. Details are discussed in Section 4.3.

Different concepts need not use the same number of neurons. If concept C is represented by θ_M , then the number of neurons used for C is $|M|$.

4.2. Sparse Autoencoder Architectures

We categorize SAE architectures into two classes: *absolute gating* and *relative gating*. In absolute gating, each neuron’s activation is determined independently of other neurons. ReLU SAE, JumpReLU SAE, and Gated SAE are examples of absolute gating. In relative gating, a neuron’s activation depends on other neurons. Top-K SAE, Matching Pursuit SAE, and SPaDE are examples of relative gating.

The geometric difference between the two mechanisms appears in the SNTA regions. In absolute gating, each neuron’s activation region is a halfspace, $N_i = H_i^+$. Thus, for ReLU SAE, $\theta_M = \bigcap_{j \in M} H_j^+$. In relative gating, a neuron can be positive but inactive because it is not selected by the competitive gating rule. For Top-K SAE,

$$N_i = \{x \in X : z_i(x) > \tau_i \text{ and } i \in \text{TopK}_k(z(x))\}.$$

Hence $N_i \subseteq H_i^+$, and N_i is generally a union of patches inside H_i^+ . An example is shown in Figure 1. Prior work describes Top-K gating regions as unions of polyhedra (Su et al., 2026; Hindupur et al., 2025). Therefore, most of our geometric results are first stated for absolute gating. For Top-K SAE, the same framework applies, but the additional relative-gating effect must be considered.

4.3. Concept Learning

For simplicity, we write θ for θ_M . Unless otherwise specified, we use *concepts* to refer to human concepts and *units* to refer to model-learned concepts. When a distinction is needed, we use *unit* for a multi-neuron activation pattern and *neuron* for the total activation region of a single neuron.

The goal of concept learning is to align human concepts \mathcal{C} with model-learned concepts Θ . We consider three levels of learning: concept detection, concept separation, and concept approximation.

4.3.1. CONCEPT DETECTION

Concept detection is the weakest form of concept learning. Its goal is to cover a selected concept. Formally, concept detection holds if $\forall C \in \mathcal{C}, \exists \theta \in \Theta$ such that $\mu(C \setminus \theta) = 0$. In SAE, this condition is often easy to satisfy because it only requires at least one unit to cover the concept. However, concept detection alone allows many-to-many mappings: one concept may be covered by multiple units, and one unit may cover multiple concepts. This motivates the stronger notions below.

4.3.2. CONCEPT SEPARATION

Concept separation asks whether a selected concept can be separated from other concepts on the observed data support.

Definition 4.1 (Concept separation). A concept C is said to be separated by θ_M if (i) $x \in H_i^+$ for all $x \in C$ and $i \in M$, and (ii) $x' \in H_j^-$ for all $x' \in X \setminus C$ and $j \in [d] \setminus M$.

Concept separation removes some ambiguity in concept detection because the selected unit must cover C exclusively. Empirically, when a single neuron is used as the concept learner, both ReLU and Top-K SAE can fail to separate complicated concepts (Hindupur et al., 2025).

The main limitation of concept separation is generalization. Since μ evaluates only observed data, θ may separate C on the training support while still including large blank regions outside that support. Thus, concept separation is useful for classification-like tasks, but it is not sufficient for novel concept discovery, where the model discovers concepts unknown to users. Novel concept discovery is especially useful in scientific domains (Singh et al., 2025; Stokes et al., 2020). The importance of novel concept discovery is also highlighted in agentic interpretability (Kim et al., 2025), where models can help users understand new concepts and correct human concept annotations (Simon & Zou, 2025).

4.3.3. CONCEPT APPROXIMATION

Concept approximation is the strongest form of concept learning. It evaluates whether a unit tightly approximates a concept in the ambient space.

Definition 4.2 (Concept approximation). A concept C is said to be approximated by θ_M if (i) $x \in H_i^+$ for all $x \in C$ and $i \in M$, and (ii) $x' \in H_j^-$ for all $x' \in \mathbb{R}^d \setminus C$ and $j \in [d] \setminus M$.

The key difference between concept separation and concept approximation is the choice of space: the former is evaluated on X , whereas the latter is evaluated in \mathbb{R}^d . Intuitively, concept approximation requires the unit to surround the concept as tightly as possible. Unlike concept separation, concept approximation can support concept discovery because it penalizes false positives and false negatives beyond the observed data. An analogue of concept approximation is anomaly detection (Ruff et al., 2018).

4.4. Neuron Interpretation

Concept learning and neuron interpretation are two directions of the same relation between concepts and units. Denote $\mathcal{N} = [d]$ as the set of neurons. Define a relation $\mathcal{R} \subseteq \mathcal{C} \times \mathcal{N}$. The relation \mathcal{R} can be interpreted as a formal context in formal concept analysis (Ganter et al., 1999). This lattice captures many-to-many correspondences between human concepts and model-learned concepts, providing a more

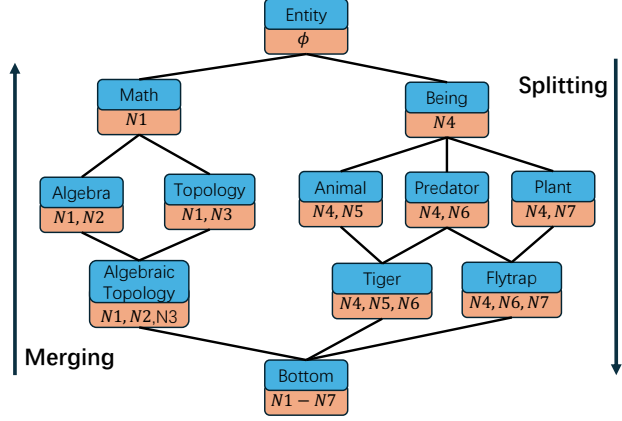


Figure 2. Toy example of a concept lattice. From top to bottom, concepts become more specific, and the associated neuron intents become more refined. From bottom to top, concepts become more general, and neuron intents are merged into coarser descriptions. structured view than selecting a single best match in either direction. An example of concept lattice can be found in Fig. 2.

4.5. Sparse Autoencoder Phenomena

We now formulate and explain several common SAE phenomena in our framework.

Polysemanticity and monosemanticity. Polysemanticity means that a neuron is related to multiple concepts. In terms of \mathcal{R} , this means that a neuron is associated with multiple unrelated concepts. Monosemanticity means that this reverse relation is concentrated on one concept, and thus requires f to be injective: different concepts should not be assigned to the same neuron. Therefore, the number of available neurons must be at least the number of concepts. This is made precise in Section 5.3.

Feature splitting. Feature splitting means that a broad neuron in a smaller SAE is split into several more specific neurons in a larger SAE. Formally, if θ is a broad neuron and $\theta_1, \dots, \theta_r$ are more specific neurons, then feature splitting can be expressed as $\theta \approx \bigcup_{j=1}^r \theta_j$ with $\theta_j \cap \theta_l \approx \emptyset$ for $j \neq l$. The approximate disjointness is consistent with sparsity: if the split neurons overlapped heavily, then data in the overlap would activate many neurons at once and violate the sparsity constraint.

Feature absorption. Feature absorption is a failure mode of hierarchical learning. Suppose $C_i \subset C_j$, where C_i is the child concept and C_j is the parent concept. Ideally, data in C_i should also activate the model concept for C_j . Absorption occurs when $\mu(C_i \cap \theta_{C_j}^c) > 0$. That is, the parent feature fails to activate on part of its child concept. This can happen because activating both parent and child features increases the sparsity cost.

Feature family. A feature family consists of several neurons that tend to activate together. Formally, a family $\theta_1, \dots, \theta_r$

has nontrivial co-activation if $\bigcap_{l=1}^r \theta_l \neq \emptyset$. These neurons may represent different aspects of the same concept or nearby concepts in a semantic family.

Hierarchical concepts. Hierarchical concepts correspond to set inclusion. If $C_i \subset C_j$, then C_i is more specific than C_j . For example, “mammal” is contained in “animal”. Ideally, the learned model concepts should satisfy $\theta_{C_i} \subset \theta_{C_j}$. However, maintaining this hierarchy can increase the sparsity cost because data in the child concept may need to activate both child and parent neurons.

5. Theoretical Results

In this section, we present the main theoretical results for concept learning and neuron interpretation, including necessary and sufficient conditions, failure conditions, and error bounds. We focus primarily on ReLU SAE and defer the corresponding results for Top-K SAE to Appendix 9.7.

We begin with the following assumption.

Assumption 5.1. \mathcal{C} has finite cardinality (i.e, there are finitely many concepts). Every concept $C \in \mathcal{C}$ is compact, and $X = \bigcup_{C \in \mathcal{C}} C$.

The finite cardinality assumption is intuitive and natural because a human cannot perceive infinitely many concepts. In \mathbb{R}^n , compact sets are closed and bounded by the Heine–Borel theorem (Munkres, 1984). This assumption is reasonable and weak: closedness means that if a data point is infinitely close to a concept, then it belongs to that concept; boundedness rules out infinite-valued data or concepts; and $X = \bigcup_{C \in \mathcal{C}} C$ ensures that every data point belongs to at least one concept. In particular, finite concepts are automatically compact. Overall, assuming concepts to be measurable and compact rules out pathological cases while still allowing flexible shapes, such as disconnected sets, Swiss rolls, and helices.

5.1. Concept Separation

We start with a simple warm-up case: using one neuron to separate a concept C . Let N denote $X \setminus C$, equivalently $\bigcup_{C' \in \mathcal{C}, C' \neq C} (C' \setminus C)$. Recall that separating C requires a neuron, or more generally a unit, to place C on its positive side and N on its negative side. The following theorem gives the necessary and sufficient condition for separation by one neuron.

Theorem 5.2 (Concept separation with one neuron). *C can be separated from N with one neuron if and only if $\text{Conv}(C) \cap \overline{\text{Conv}(N)} = \emptyset$, where Conv denotes the convex hull.*

The proof can be found in Appendix 9.4.1. If we use one neuron for each concept to separate all concepts, the following two corollaries follow immediately.

Corollary 5.3. *1. All concepts in \mathcal{C} can be separated from each other if and only if $\text{Conv}(C_i) \cap \overline{\text{Conv}(N_i)} = \emptyset$ for all $C_i \in \mathcal{C}$.*

2. When concept separation is possible for \mathcal{C} , the minimum number of selected neurons is $|\mathcal{C}|$.

The proof can be found in Appendix 9.4.2. These results show that concept separation with a single neuron is highly demanding. Corollary 5.3 also clarifies a difficulty in neuron interpretation: monosemanticity is hard to achieve because concepts in LLM activation spaces can be twisted, and their convex hulls are unlikely to be disjoint. Despite this difficulty, SAEs can mitigate polysemanticity because (1) they introduce more neurons as candidates for concept separation, as shown below, and (2) concepts that can be inherently disentangled or split may satisfy these requirements. Our proofs are constructive; training an SAE is not guaranteed to find such constructions, but having more neurons increases the chance of successful separation.

We next consider separation by multiple neurons, or a unit. In this case, the requirements can be weaker:

Theorem 5.4 (Concept separation with multiple neurons). *C can be separated from N by a unit if and only if $\text{Conv}(C) \cap \overline{N} = \emptyset$.*

The proof can be found in Appendix 9.4.3. The corresponding corollaries for separating all concepts with units are as follows.

Corollary 5.5. *All concepts in \mathcal{C} can be separated from each other by units if and only if $\text{Conv}(C_i) \cap \overline{(C_j \setminus C_i)} = \emptyset$ for all $C_i \in \mathcal{C}$ and $C_j \neq C_i \in \mathcal{C}$.*

The proof can be found in Appendix 9.4.4. These results show that unit-based concept separation has much weaker requirements than neuron-based separation, leading to cleaner concept learning and more disentangled neuron interpretation. For example, with a single neuron, a concept cannot be separated when other concepts surround it; with a unit, such separation may still be possible. One consequence is that feature splitting is not universal across all concepts, and hierarchical concepts can be difficult to learn without architectural changes.

Although the above results are primarily built on finite-dimensional spaces, we maintain flexibility to extend to infinite-dimensional spaces, as discussed in Appendix 9.4.1.

When perfect separation is not possible, we need to study the resulting error. We define the separation error as follows.

Definition 5.6 (Separation error). The separation error is the symmetric difference on the data support:

$$e_{sep}(C, \theta) = \mu(C \Delta \theta) = \underbrace{\mu(\theta \setminus C)}_{\text{contamination error } e_c} + \underbrace{\mu(C \setminus \theta)}_{\text{missing error } e_m},$$

where μ is a Borel probability measure supported on X .

This definition also applies when θ is a single neuron. Intuitively, e_m measures how much of the target concept is missed by the selected unit, while e_c measures how much unrelated content is covered by the selected unit, leading to polysemanticity. Variants of separation error are discussed in Appendix 9.4.5. The separation error is zero when perfect separation holds up to a μ -null set. In non-separable concept learning, however, it cannot reach zero and has an irreducible component.

When concepts are not disjoint, separation on the overlapping boundary reduces to concept approximation, which we discuss next.

5.2. Concept Approximation

We define the approximation error as follows.

Definition 5.7 (Approximation error). The approximation error is the symmetric difference under the ambient measure:

$$e_{app}(C, \theta) = \nu(C \Delta \theta),$$

where ν is a Borel probability measure supported on \mathbb{R}^n .

Unlike concept separation, which considers only observed data, concept approximation must also account for novel data. Although a single neuron may separate concepts on the observed support, it is generally insufficient for concept approximation. We therefore focus on multi-neuron activations, or units. The necessary and sufficient condition is as follows.

Theorem 5.8 (Concept approximation condition). *A concept $C \in \mathcal{C}$ can be arbitrarily well approximated under the approximation error by a unit if and only if C is convex up to a ν -null set.*

The proof can be found in Appendix 9.5.1. Thus, for all concepts to be arbitrarily well approximated by units, each concept must be convex up to a ν -null set. The error rate is given by the following theorem.

Theorem 5.9 (Concept approximation error rate). *Under regularity and boundary-smoothness conditions, a concept $C \in \mathcal{C}$ can be approximated by a unit θ_M with error*

$$e_{app}(C, \theta_M) \lesssim e_{irr} + A|M|^{-\frac{2}{r-1}},$$

where A is a constant related to boundary smoothness, r is the effective dimension of C , and e_{irr} is an irreducible error. In particular, $e_{irr} = 0$ when C is convex, or more generally when $\nu(\text{Conv}(C) \setminus C) = 0$.

Details and proofs can be found in Appendix 9.5.2. Intuitively, the irreducible error is nonzero when C is non-convex to a positive degree, because a unit is essentially a

convex polytope and therefore cannot eliminate the penalty from non-convexity. To approximate all concepts arbitrarily well, each concept must be convex, and the number of neurons must satisfy $d \geq \sum_{i=1}^{|C|} |M_i|$ when θ_{M_i} is used to approximate C_i ; this lower bound can be reduced when neurons are reused across concepts. Although concept approximation appears stricter than concept separation and requires more neurons, perfect concept approximation can impose weaker structural requirements in cases where concepts overlap: overlapping convex concepts can be approximated arbitrarily well, whereas concept separation is impossible in this setting. The larger neuron requirement in concept approximation helps exclude unrelated regions and better resolve polysemanticity.

Note that although the above theories for concept separation and concept approximation are for concept learning, they also apply to neuron interpretation because the selected neuron/unit forms an exclusive relation with the target concept, so the interpretation of the neuron/unit corresponds to the target concept.

5.3. Concept Learning Capacity

To make monosemanticity possible, the selected concept learning function f should be approximately injective. This yields a necessary combinatorial capacity condition.

Without loss of generality, let d be the number of non-dead neurons. Let k_c be the maximum number of neurons allowed to represent a concept C . The value of k_c is an interpretation budget; for Top-K SAE, one should have $k_c \leq k$, where k is the Top-K sparsity.

Theorem 5.10 (Concept learning capacity). *Suppose perfect monosemanticity holds for all concepts, and each concept is represented by at most k_c neurons. In the regime $d \gg k_c$, this requires approximately*

$$d \gtrsim (k_c! |\mathcal{C}|)^{1/k_c}. \quad (5)$$

The proof can be found in Appendix 9.6. This is a necessary condition and does not by itself guarantee concept separation or approximation. Although it may appear to contradict Corollary 5.3, Corollary 5.5, and Theorem 5.8, those earlier results do not account for sparsity, whereas sparsity is explicitly considered here.

5.4. Concept Learning and Neuron Interpretation

Although neuron interpretation has not been specified in the previous sections, the theoretical results above still provide insight into it. In particular, using individual neurons or multi-neuron units for concept learning leads to different levels of interpretation quality, such as different degrees of monosemanticity. We now state the link between concept learning and neuron interpretation in an algebraic way.

Define U as the power set of all data, $U = \mathcal{P}(X)$, so that the human concept family \mathcal{C} is a finite subset of U . Recall that $\mathcal{N} = [d]$ is the set of neurons and $M \in \mathcal{P}(\mathcal{N})$ is a set of neurons and $\theta_M \subseteq X$ is the activation region of M . For a single neuron $N \in \mathcal{N}$, we write $\theta_N := \theta_{\{N\}}$. Since each θ_M is a subset of X , we also regard it as an element of U .

We define a binary relation $R \subseteq U \times \mathcal{N}$ by

$$CRN \iff C \subseteq \theta_N.$$

Intuitively, CRN means that neuron N is active on the whole data region C . When $C \in \mathcal{C}$, this says that N covers the whole human concept region C . This relation is not assumed to be a function: a concept may be represented by multiple neurons, and a neuron may be related to multiple concepts.

The relation R induces two maps

$$\begin{aligned} f : U &\rightarrow \mathcal{P}(\mathcal{N}), & f(C) &= \{N \in \mathcal{N} : CRN\}, \\ g : \mathcal{P}(\mathcal{N}) &\rightarrow U, & g(M) &= \bigcap_{N \in M} \theta_N, \end{aligned}$$

with the convention that $g(\emptyset) = X$. The map f sends a data region to the set of neurons that are active on the entire region. Thus, f corresponds to the concept-to-neuron direction. The map g sends a set of neurons to their common activation region. Thus, g corresponds to the neuron-to-region direction used in neuron interpretation.

Due to space limit, we put the complete results in Appendix 9.3. The complete results contains construction of concept lattice and algebraic explanations of SAE phenomena.

6. Experiments

Our theoretical results are constructive. In a trained SAE, however, the neurons are fixed, so concept learning becomes a search problem over the learned model-concept set:

$$\theta_C^* = \arg \min_{\theta \in \Theta} \text{metric}(C, \theta), \quad (6)$$

where metric is a task-dependent loss, such as separation or approximation error. For score-based metrics such as F1, we equivalently maximize the score. Thus, the constructive results characterize when concept learning is possible in principle, while the empirical setting measures how well the trained neurons approximate the constructive results. Our experiments study how concept learning quality changes with the number of selected neurons, SAE expansion factor, and SAE sparsity. In particular, we ask whether larger SAEs provide more candidate features for representing a concept, and whether concept learning and neuron interpretation induce the same feature–concept correspondence. We empirically study Corollaries 5.3 and 5.5, Theorems 5.9 and 5.10, and Section 4.4.

6.1. Setup

Data and Model. We use two-dimensional synthetic data for ease of visualization and analysis. Each human concept is represented by a cluster in the input space. This controlled setting lets us directly compare the geometry of human concepts with the model concepts induced by SAE features. We consider two data configurations: mutually disjoint concepts and partially overlapping concepts. We train ReLU SAEs and Top- K SAEs while varying expansion factor and sparsity. All models are trained until convergence. Details are provided in Appendix 9.2.

Metrics. Following Hindupur et al. (2025), we use F1 score as the primary metric. To obtain a more complete view of concept-learning quality, we also report the separation error e_{sep} and approximation error e_{approx} in the case study in Section 7.3.

Neuron Selection Algorithms. For an SAE with target sparsity $L_0 = k$, we evaluate units containing at most k selected neurons. Selecting an SAE feature subset, or equivalently a set of hyperplanes, to optimize a target metric is combinatorial. Exhaustive search quickly becomes infeasible: for example, choosing exactly 8 features from an SAE of width 64 requires evaluating $\binom{64}{8} = 4,426,165,368$ candidate subsets. We therefore use heuristic selection. In the main results, we report top- N selection, which is closest to common interpretability practice: features are ranked by their score for the target concept, and the top N features are selected to form the unit. Unless stated otherwise, the x-axis reports the exact number N of selected neurons; when reporting a best score, we optimize over feasible $N \leq k$.

6.2. Results

The theory suggests that enlarging the candidate set—through a larger expansion factor, a higher L_0 , or a larger selection budget—should improve the chance of finding a good concept learner. However, exact- N performance need not be monotone. We therefore study how F1 score and disagreement ratio depend on SAE size, sparsity, and the number of selected neurons.

We present the results for ReLU SAEs and Top- K SAEs in Fig. 3 and Fig. 4, respectively.

6.2.1. CONCEPT SEPARATION AND APPROXIMATION

To study the effect of the number of selected neurons, we fix expansion factor 8 for panels (a)–(h) in Fig. 3 and Fig. 4. For each concept, we plot one curve per L_0 . In the discussion below, we report the L_0 curve that achieves the best F1 score in the corresponding panel.

For a neuron-separable concept (panels (a),(b)), both ReLU and Top- K SAEs can separate the concept with a single

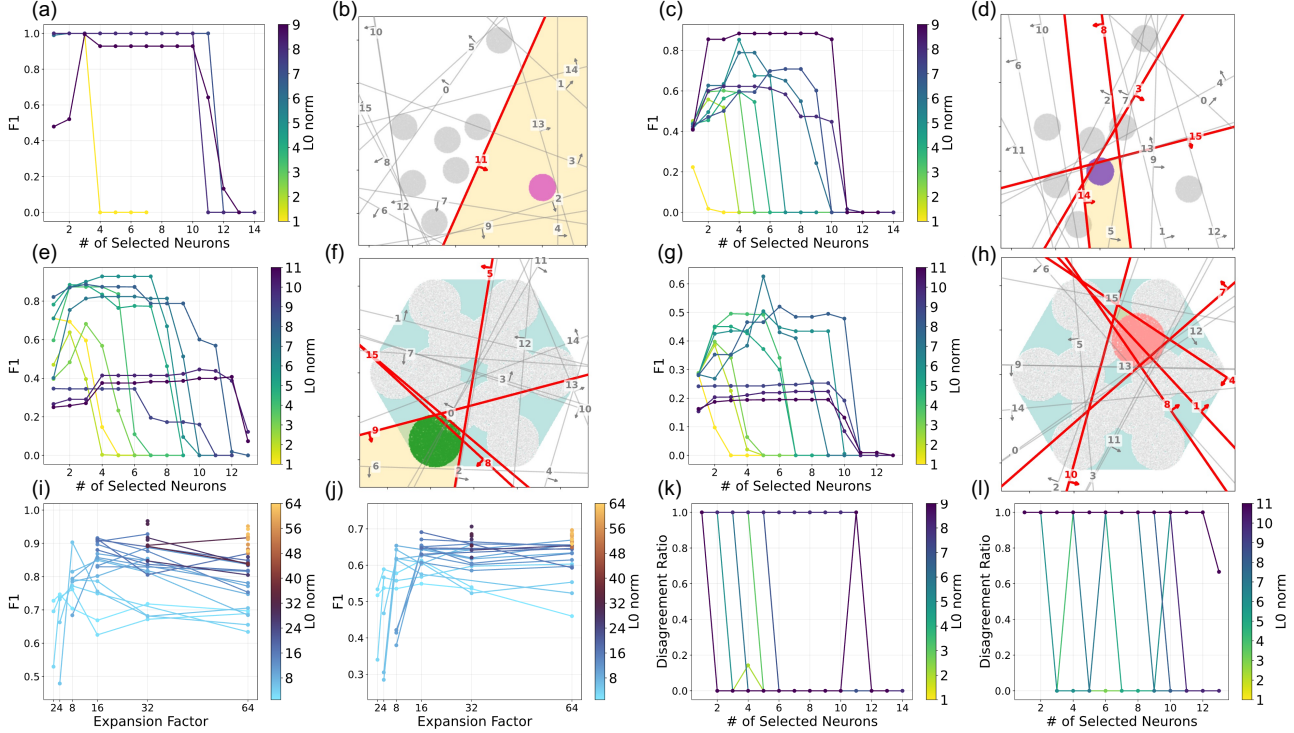


Figure 3. Concept separation, concept approximation, concept-learning capacity, and concept learning–neuron interpretation disagreement for ReLU SAEs. Panels (a)–(h) and (k)–(l) use expansion factor 8; panels (i)–(j) vary the expansion factor. **(a)(b):** F1 score and visualization for a neuron-separable concept (Theorem 5.2). **(c)(d):** F1 score and visualization for a non-neuron-separable but unit-separable concept (Theorem 5.4). **(e)(f):** approximation F1 score and visualization for an easier-to-approximate concept (Theorems 5.8 and 5.9); the blue region inside the convex hull of all concepts represents novel/unseen data. **(g)(h):** approximation F1 score and visualization for a harder-to-approximate concept. **(i)(j):** concept-learning capacity, measured by the best F1 score (Theorem 5.10), on disjoint and overlapping concepts. **(k)(l):** concept learning–neuron interpretation disagreement ratio (Section 4.4) for the selected concepts in (d) and (h).

neuron, achieving perfect F1. For a non-neuron-separable but unit-separable concept (panels (c),(d)), multi-neuron units substantially improve performance. In the ReLU SAE at $L_0 = 5$, F1 increases from 0.4144 with one neuron to 0.8529 with a 4-neuron unit. In the Top- K SAE at $L_0 = 6$, F1 increases from 0.4559 to 0.9646 with a 3-neuron unit. Although the learned units are not always perfect, the visualizations show that intersecting multiple neurons yields more exclusive activation regions and can represent more complex concepts than a single neuron.

Panels (e)–(h) study concept approximation with overlapping concepts and novel/unseen probe regions. Concept clusters are shown as circles. The blue region is the convex hull of all concepts after excluding seen concept regions; we use a soft boundary, treating points within the 95th-percentile distance to a concept cluster as seen. Panels (e),(f) show an easier-to-approximate concept that overlaps with only one other concept. In the ReLU SAE at $L_0 = 6$, F1 increases from 0.710 with one neuron to 0.9281 with a 4-neuron unit. In the Top- K SAE at $L_0 = 4$, F1 increases from 0.7815 to 0.9089 with a 5-neuron unit. Panels (g),(h) show a harder-to-approximate concept that overlaps with

three other concepts. In the ReLU SAE at $L_0 = 7$, F1 increases from 0.2829 with one neuron to 0.6261 with a 5-neuron unit; in the Top- K SAE, the best multi-neuron unit reaches a substantially higher F1 than any single neuron, but still remains below the easier approximation case. These results show that a single neuron is generally insufficient for concept approximation, and that multi-neuron units improve approximation but do not eliminate the difficulty of heavy overlap.

The visualizations also clarify the difference between separation and approximation. Concept separation only needs to separate observed concepts, so its learned regions may remain unbounded. Concept approximation must also exclude novel/unseen regions, so the learned unit tends to shrink and bound the target concept more tightly. This is most visible when comparing panels (f) and (h): as the target concept overlaps more heavily with others, the unit becomes more closed around the target.

We also observe that F1 is not monotone in the exact number of selected neurons: it often first increases and then drops to zero when too many neurons are selected. We analyze this phenomenon in Section 7.2. We further analyze the differ-

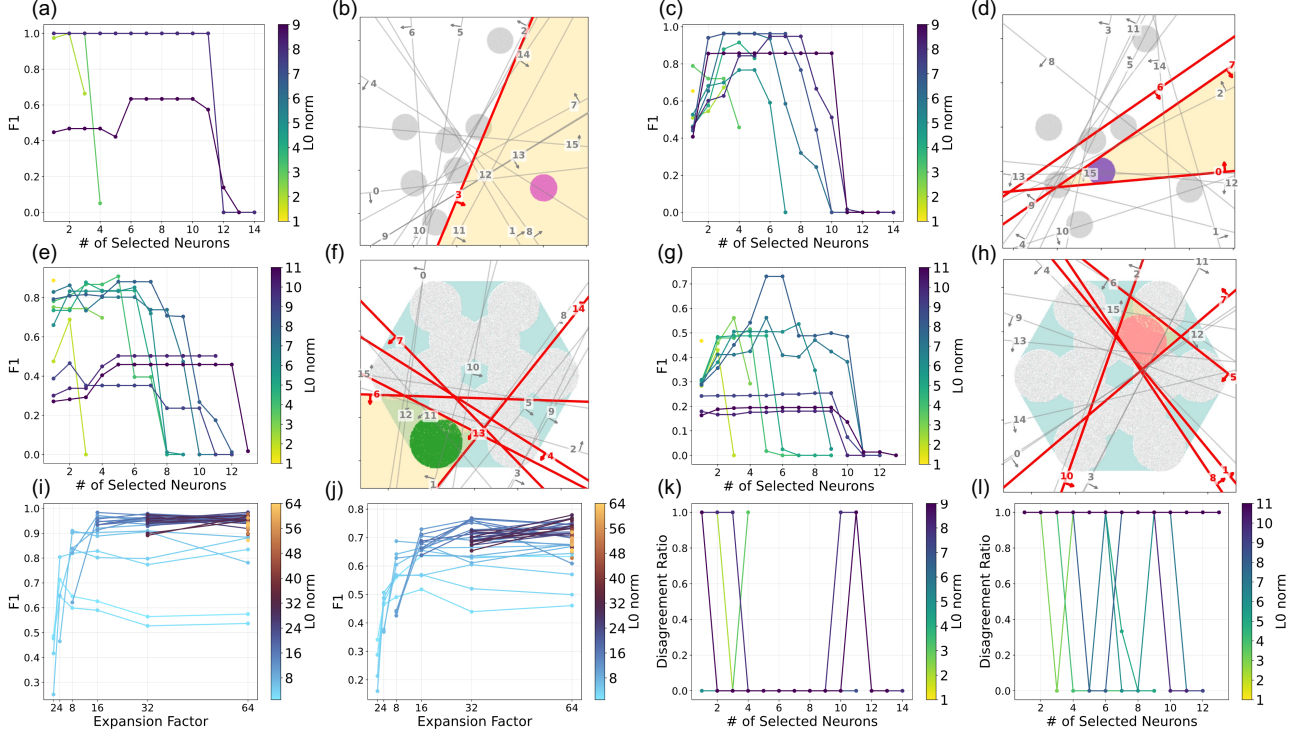


Figure 4. Concept separation, concept approximation, concept-learning capacity, and concept learning–neuron interpretation disagreement for Top- K SAEs. Panels (a)–(h) and (k)–(l) use expansion factor 8; panels (i)–(j) vary the expansion factor. (a)(b): F1 score and visualization for a neuron-separable concept (Theorem 5.2). (c)(d): F1 score and visualization for a non-neuron-separable but unit-separable concept (Theorem 5.4). (e)(f): approximation F1 score and visualization for an easier-to-approximate concept (Theorems 5.8 and 5.9); the blue region inside the convex hull of all concepts represents novel/unseen data. (g)(h): approximation F1 score and visualization for a harder-to-approximate concept. (i)(j): concept-learning capacity, measured by the best F1 score (Theorem 5.10), on disjoint and overlapping concepts. (k)(l): concept learning–neuron interpretation disagreement ratio (Section 4.4) for the selected concepts in (d) and (h).

ence between separation and approximation in Section 7.1.

6.2.2. CONCEPT LEARNING CAPACITY

To study the effect of expansion factor on concept-learning capacity, we aggregate each concept by taking the number of selected neurons that achieves the best F1 score, and then plot one curve per L_0 . We use this best F1 score as an operational measure of capacity: a higher-capacity SAE should separate or approximate concepts more accurately. Panels (i),(j) in Fig. 3 and Fig. 4 show the results.

For ReLU SAEs, increasing the expansion factor from 2 to 16 substantially improves F1 at fixed L_0 , after which the gains plateau. This is expected: larger SAEs provide a larger pool of candidate neurons, but once useful feature combinations are available, additional width brings diminishing returns. The plateau is even clearer for Top- K SAEs. Disjoint concepts are easier to learn than overlapping concepts, as reflected by their higher peak F1 scores. At fixed expansion factor, larger L_0 generally improves F1 because each concept can use a larger selection budget.

6.2.3. NEURON INTERPRETATION

To study concept learning–neuron interpretation disagreement, we again choose, for each concept, the number of selected neurons that gives the best F1 score, and then compute the corresponding disagreement ratio. We plot one curve per L_0 in panels (k),(l) of Fig. 3 and Fig. 4. For a target concept A , let

$$\theta^* = \arg \max_{\theta \in \Theta} s(A, \theta),$$

$$B = \arg \max_{C \in \mathcal{C}} s(C, \theta^*),$$

$$\text{Disagree} = \mathbf{1}\{A \neq B\},$$

where s is the F1 score. The first two lines correspond to the forward concept-learning map f and the reverse neuron-interpretation map g in Section 4.4. The disagreement ratio averages this indicator over concepts. When $A = B$, the target concept and its selected unit form a fixed point of the Galois connection, i.e., a formal concept in the concept lattice.

Panels (k),(l) study the disagreement ratio for the separation example in (d) and the approximation example in (h). Com-

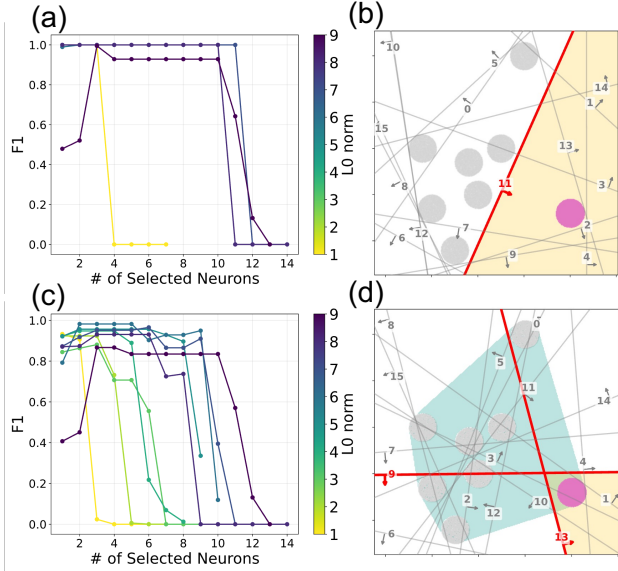


Figure 5. Difference between concept separation and concept approximation, with expansion factor 8. (a)(b): F1 score and visualization for a neuron-separable concept under concept separation; one neuron at $L_0 = 1$ achieves F1= 1.0. (c)(d): F1 score and visualization for the same concept under concept approximation; the best case shown uses $L_0 = 6$ and achieves F1= 0.9281.

paring (c) with (k), and (g) with (l), lower but nonzero F1 generally corresponds to higher disagreement, while high F1 gives low disagreement. This matches the role of F1 as a membership-exclusivity metric. Comparing (k) and (l), overlapping concepts produce more disagreement than disjoint concepts, because the reverse map can easily select a nearby overlapping concept. A zero F1 score can sometimes yield no disagreement when too many selected neurons make the intersection empty or nearly empty; under our convention, the reverse step then selects the target concept or no competing concept.

Overall, these results show that concept learning and neuron interpretation need not agree. We discuss this mismatch in more detail in Section 7.4.

7. Analysis

7.1. Difference Between Concept Separation and Approximation

Although concept separation and concept approximation are mathematically related, they behave differently in practice. Fig. 5 shows a case study on the same neuron-separable concept. Under concept separation, one neuron perfectly separates the target concept (F1= 1.0). Under concept approximation, perfect F1 is not achieved; the best unit shown reaches F1= 0.9281.

The difference comes from what each task penalizes. Concept separation is evaluated only on observed data support,

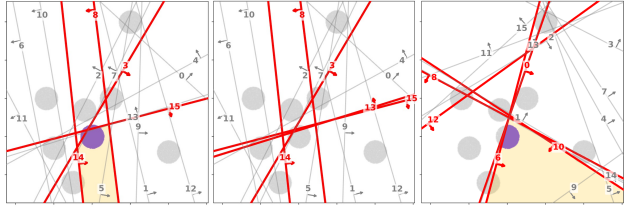


Figure 6. Visualizations of concept separation with different exact numbers of selected neurons. Left: best unit for $L_0 = 5$ with $N = 4$ selected neurons, achieving F1= 0.8529. Middle: the same SAE with $N = 5$, where F1 drops to 0.0924. Right: best unit with exact $N = 5$, achieving F1= 0.6748.

so the learner only needs to include the target concept and exclude other observed concepts. Concept approximation also evaluates novel/unseen regions, so the unit must bound the target concept more tightly and avoid over-generalizing into blank regions. This explains why approximation uses more neurons in Fig. 5(d), and why its F1 curves resemble the harder multi-neuron cases in Fig. 3 and Fig. 4. It also supports the observation from Section 5.1: when concepts overlap, separation on the boundary begins to behave like approximation.

7.2. More Selected Neurons Is Not Monotonically Better

In Fig. 3 and Fig. 4, increasing the exact number of selected neurons does not always increase F1. This does not contradict Corollary 5.5: the theory says that a larger neuron budget gives more freedom, not that a concept must benefit from using more neurons.

Fig. 6 illustrates the issue. The left panel shows the best unit for $L_0 = 5$ with $N = 4$ selected neurons. If we keep the same SAE and force one more selected neuron, the activation region can shrink sharply and cut out most of the target concept, causing the F1 drop shown in the middle panel. Even after re-optimizing the selection for exact $N = 5$ (right panel), the best F1 remains below the $N = 4$ optimum. Thus, exact- N curves can decrease because additional intersections may remove useful parts of the target concept. If the x-axis instead represented “up to N ” selected neurons, the curve would be non-decreasing, since the learner could always reuse the best smaller unit.

7.3. Illusions of Separation/Approximation Error & Limitations of Top- K Selection

Although $e_{\text{sep}} = 0$ and $e_{\text{app}} = 0$ characterize perfect concept separation and approximation, these errors can be poor objectives for selecting neurons. Fig. 7 shows a representative failure case.

The left panel may appear benign because several curves remain close to zero. However, for $L_0 = 6$, increasing the number of selected neurons from 2 to 3 makes the activation region miss the target concept almost entirely (middle and

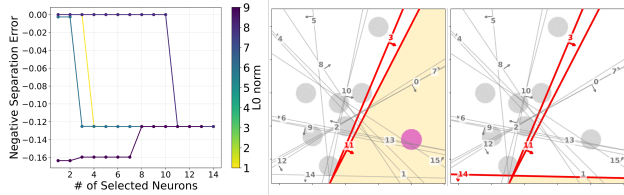


Figure 7. Negative separation error and visualizations when $-e_{\text{sep}}$ is used as the neuron-selection objective, with expansion factor 8. *Left*: $-e_{\text{sep}}$ versus the number of selected neurons. *Middle*: best 2-neuron unit for $L_0 = 6$, with $-e_{\text{sep}} = -0.0026$. *Right*: best 3-neuron unit for $L_0 = 6$, with $-e_{\text{sep}} = -0.1253$.

right panels). The heuristic selects neuron 14 because it has small separation error: it misses target mass 0.12 but has zero contamination. For small target concepts, missing the target can therefore be penalized less than including unrelated concepts.

This is a class-imbalance effect, which has been studied intensively in anomaly detection (Ruff et al., 2018). Each concept occupies only a small part of the total space, so treating concept learning as binary classification with an unnormalized measure can favor conservative solutions that reject the target concept rather than risk false positives. Measure-weighted errors also underweight small concepts: if $\mu(C_1) = 0.2$ and $\mu(C_2) = 0.01$, then completely missing C_2 incurs a much smaller penalty than missing C_1 . This suggests that concept learning and neuron interpretation need metrics that normalize by concept mass, such as F1 score or Intersection-over-Union (IoU). This issue is related to the metric sanity checks studied in Oikarinen et al. (2025). We omit separate IoU results because they are qualitatively similar to the F1 results reported above. Analytically, the corresponding IoU error has the same asymptotic approximation rate as the approximation error, up to an additional $1/\mu(C)$ factor; this factor gives relatively more weight to small-mass concepts.

Finally, Fig. 7 also shows a limitation of top- N selection. For $N = 3$, the better combination is neurons (3, 11, 0), but neuron 0 has large individual contamination error and is not selected; the heuristic instead selects neuron 14, which looks good individually but destroys the intersection. Thus, a neuron can be poor alone but useful in combination. This score-wise greediness can break top- N selection, and similar failures can occur in other greedy methods, including matching pursuit (Wang et al., 2012; Costa et al., 2025) and forward selection (Borboudakis & Tsamardinos, 2019).

7.4. More About Disagreement Ratio

Table 1 gives a broader view of how disagreement depends on expansion factor, concept type, learning task, and SAE architecture. Four trends stand out. First, disjoint concepts yield lower disagreement than overlapping concepts. Second, concept separation usually yields lower disagreement

than concept approximation. Third, on disjoint concepts, Top- K SAEs are worse than ReLU SAEs at small expansion factors but catch up or improve at larger expansion factors; on overlapping concepts, Top- K SAEs are generally less stable. Fourth, increasing the expansion factor reduces disagreement.

The first two trends follow from concept-learning quality. Disjoint concepts and separation tasks usually achieve higher F1 scores, meaning that the learned unit captures the target concept more exclusively; this lowers the chance that the reverse neuron-interpretation map selects another concept. Approximation is harder because unseen and unapproximatable regions create additional ambiguity. The fourth trend is also expected: a larger expansion factor gives a larger pool of candidate neurons and allows activation regions to surround the data support more flexibly.

The architectural trend is more subtle. For Top- K SAEs, activation regions are subsets of the corresponding ReLU halfspaces because a neuron can have positive pre-activation but still fail to enter the top- K set. This relative gating creates “holes” in activation regions. On disjoint concepts, such holes are less likely to intersect relevant data support, so the main effect of Top- K gating is to suppress weak residual activations; at larger expansion factors this can produce cleaner features and lower disagreement. On overlapping concepts, however, the holes are more likely to fall inside data support, which destabilizes the reverse map and can increase disagreement. Thus, Top- K competition gives cleaner sparsity but may reduce the stability of the concept lattice when concepts overlap.

Table 2 further shows that disagreement is concentrated at intermediate F1 scores. In this regime, a neuron or unit partially learns the target concept while also mixing in other concepts. High F1 scores, especially F1=1, almost never produce disagreement. This supports the use of F1 as a practical metric for concept learning because it directly rewards membership exclusivity.

Since real-world concepts are often overlapping rather than disjoint, future work should account for overlap when choosing the SAE architecture, concept-learning objective, and neuron-selection algorithm.

8. Discussion

In this work, we propose a mathematical framework for studying concept learning and neuron interpretation in sparse autoencoders. We formulate human and model concepts as sets, and view concept learning as a problem of set alignment. This perspective distinguishes three modes of alignment: concept detection, concept separation, and concept approximation, each capturing a different relationship between human concepts and SAE-induced model concepts.

A Geometric View for Understanding Concept Learning and Neuron Interpretation in Sparse Autoencoders

Concept Type	Concept Learning Type	SAE Architecture	EF=2	EF=4	EF=8	EF=16	EF=32	EF=64
Disjoint Concepts	Concept Separation	ReLU	0.44	0.26	0.17	0.04	0.02	0.01
		Top-K	0.70	0.36	0.14	0.03	0.01	0.01
	Concept Approximation	ReLU	0.51	0.33	0.24	0.12	0.06	0.05
		Top-K	0.72	0.41	0.23	0.08	0.03	0.03
Overlapping Concepts	Concept Separation	ReLU	0.69	0.52	0.45	0.28	0.25	0.22
		Top-K	0.82	0.66	0.41	0.31	0.30	0.31
	Concept Approximation	ReLU	0.69	0.52	0.45	0.29	0.23	0.20
		Top-K	0.82	0.66	0.42	0.31	0.28	0.30
All			0.69	0.50	0.31	0.15	0.12	0.10

Table 1. Disagreement ratio by concept type, concept-learning task, SAE architecture, and expansion factor (EF). Each cell reports the disagreement ratio after optimizing F1. For each concept, we choose the number of selected neurons that gives the best F1 score, average over L_0 and seeds, and then average over concepts.

Concept Type	Concept Learning Type	SAE Architecture	=0	(0,.2]	(.2,.4]	(.4,.6]	(.6,.8]	(.8,1)	=1
Disjoint Concepts	Concept Separation	ReLU	0.07	0.74	0.86	0.46	0.22	0.00	0.00
		Top-K	–	1.00	0.79	0.49	0.15	0.00	0.00
	Concept Approximation	ReLU	0.07	0.77	0.75	0.43	0.04	0.00	–
		Top-K	–	0.81	0.75	0.42	0.03	0.00	–
Overlapping Concepts	Concept Separation	ReLU	0.05	0.54	0.79	0.79	0.00	0.00	–
		Top-K	–	0.89	0.82	0.73	0.00	0.00	–
	Concept Approximation	ReLU	0.05	0.61	0.83	0.66	0.00	0.00	–
		Top-K	–	0.90	0.81	0.61	0.00	0.00	–
All			0.05	0.72	0.81	0.66	0.04	0.00	0.00

Table 2. Disagreement ratio by F1 interval. Each cell reports the disagreement ratio for cases whose optimized F1 score falls in the corresponding interval. The optimized unit size is chosen per concept, and values are averaged over L_0 , seeds, and concepts.

Our analysis explains several phenomena in SAE-based interpretability. In particular, it shows why a single neuron is often insufficient for representing a human concept, why wider SAEs can improve concept learning by providing more candidate features, and why excessive sparsity may hurt when a concept requires multiple features. We also derive capacity and data geometry requirements for successful concept learning, linking concept geometry and SAE width.

Finally, we show that concept learning and neuron interpretation are not equivalent. A feature set may represent a human concept well in the forward direction, but need not be uniquely associated with that concept in the reverse direction. This discrepancy suggests the need for metrics and algorithms that capture bidirectional alignment and the set geometry of concepts.

This work has several limitations. First, our theoretical analysis focuses primarily on ReLU SAEs, while SAEs with gated activations or other architectural variants are not fully studied. Second, although we identify a discrepancy between concept learning and neuron interpretation, we do not yet provide a rigorous concept-lattice formulation that characterizes their bidirectional relationship, and our empirical study of this relationship remains preliminary. Future work can develop a more general formulation of both problems, study richer SAE architectures and data geometries, and design algorithms that reach agreement between concept learning and neuron interpretation.

References

Aliprantis, C. D. and Border, K. C. *Infinite Dimensional Analysis: a Hitchhiker’s Guide*. Springer, Berlin; London, 2006. ISBN 9783540326960 3540326960. doi: 10.1007/3-540-29587-9.

Anwar, U., Saparov, A., Rando, J., Paleka, D., Turpin, M., Hase, P., Lubana, E. S., Jenner, E., Casper, S., Sourbut, O., et al. Foundational challenges in assuring alignment and safety of large language models. *arXiv preprint arXiv:2404.09932*, 2024a.

Anwar, U., Saparov, A., Rando, J., Paleka, D., Turpin, M., Hase, P., Lubana, E. S., Jenner, E., Casper, S., Sourbut, O., et al. Foundational challenges in assuring alignment and safety of large language models. *arXiv preprint arXiv:2404.09932*, 2024b.

Ayonrinde, K. and Jaburi, L. A mathematical philosophy of explanations in mechanistic interpretability—the strange science part ii. *arXiv preprint arXiv:2505.00808*, 2025.

Bhalla, U., Fel, T., Rager, C., Feucht, S., Haklay, T., Wurgaft, D., Boppana, S., Kowal, M., Shyam, V., Merullo, J., et al. Do sparse autoencoders capture concept manifolds? *arXiv preprint arXiv:2604.28119*, 2026.

Bills, S., Cammarata, N., Mossing, D., Tillman, H., Gao, L., Goh, G., Sutskever, I., Leike, J., Wu, J., and Saunders, W. Language models can explain neurons in language models. <https://>

- [//openaipublic.blob.core.windows.net/neuron-explainer/paper/index.html](https://openaipublic.blob.core.windows.net/neuron-explainer/paper/index.html), 2023.
- Borboudakis, G. and Tsamardinos, I. Forward-backward selection with early dropping. *Journal of Machine Learning Research*, 20(8):1–39, 2019. URL <http://jmlr.org/papers/v20/17-334.html>.
- Bricken, T., Templeton, A., Batson, J., Chen, B., Jermyn, A., Conerly, T., Turner, N., Anil, C., Denison, C., Askell, A., et al. Towards monosemanticity: Decomposing language models with dictionary learning. *Transformer Circuits Thread*, 2(5):6, 2023.
- Chanin, D., Wilken-Smith, J., Dulka, T., Bhatnagar, H., Golechha, S., and Bloom, J. A is for absorption: Studying feature splitting and absorption in sparse autoencoders. *arXiv preprint arXiv:2409.14507*, 2024.
- Costa, V., Fel, T., Lubana, E. S., Tolooshams, B., and Ba, D. From flat to hierarchical: Extracting sparse representations with matching pursuit. *arXiv preprint arXiv:2506.03093*, 2025.
- Cunningham, H., Ewart, A., Riggs, L., Huben, R., and Sharkey, L. Sparse autoencoders find highly interpretable features in language models. *arXiv preprint arXiv:2309.08600*, 2023.
- DeGrave, A. J., Janizek, J. D., and Lee, S.-I. Ai for radiographic covid-19 detection selects shortcuts over signal. *Nature Machine Intelligence*, 3(7):610–619, 2021.
- Elhage, N., Nanda, N., Olsson, C., Henighan, T., Joseph, N., Mann, B., Askell, A., Bai, Y., Chen, A., Conerly, T., et al. A mathematical framework for transformer circuits. *Transformer Circuits Thread*, 1(1):12, 2021.
- Elhage, N., Hume, T., Olsson, C., Schiefer, N., Henighan, T., Kravec, S., Hatfield-Dodds, Z., Lasenby, R., Drain, D., Chen, C., et al. Toy models of superposition. *arXiv preprint arXiv:2209.10652*, 2022.
- Fel, T., Franchi, G., et al. A geometric unification of concept learning with concept cones. *arXiv preprint arXiv:2512.07355*, 2025.
- Gadgil, S., Lin, C., and Lee, S.-I. Ensembling sparse autoencoders. *arXiv preprint arXiv:2505.16077*, 2025.
- Ganter, B., Wille, R., and Wille, R. *Formal concept analysis*, volume 150. Springer, 1999.
- Gao, L., la Tour, T. D., Tillman, H., Goh, G., Troll, R., Radford, A., Sutskever, I., Leike, J., and Wu, J. Scaling and evaluating sparse autoencoders. *arXiv preprint arXiv:2406.04093*, 2024.
- Gurnee, W., Nanda, N., Pauly, M., Harvey, K., Troitskii, D., and Bertsimas, D. Finding neurons in a haystack: Case studies with sparse probing. *arXiv preprint arXiv:2305.01610*, 2023.
- Heap, T., Lawson, T., Farnik, L., and Aitchison, L. Sparse autoencoders can interpret randomly initialized transformers. *arXiv e-prints*, pp. arXiv–2501, 2025.
- Hindupur, S. S. R., Lubana, E. S., Fel, T., and Ba, D. Projecting assumptions: The duality between sparse autoencoders and concept geometry. *arXiv preprint arXiv:2503.01822*, 2025.
- Kim, B., Hewitt, J., Nanda, N., Fiedel, N., and Tafjord, O. Because we have llms, we can and should pursue agentic interpretability. *arXiv preprint arXiv:2506.12152*, 2025.
- Koh, P. W., Nguyen, T., Tang, Y. S., Mussmann, S., Pierson, E., Kim, B., and Liang, P. Concept bottleneck models. In *International conference on machine learning*, pp. 5338–5348. PMLR, 2020.
- Leask, P., Bussmann, B., Pearce, M. T., Bloom, J. I., Tigges, C., Al Moubayed, N., Sharkey, L., and Nanda, N. Sparse autoencoders do not find canonical units of analysis. In *The Thirteenth International Conference on Learning Representations*, 2025.
- Ludwig, M. Asymptotic approximation of smooth convex bodies by general polytopes. *Mathematika*, 46(1): 103–125, 1999. doi: 10.1112/S0025579300007609.
- Michaud, E. J., Gorton, L., and McGrath, T. Understanding sparse autoencoder scaling in the presence of feature manifolds. *arXiv preprint arXiv:2509.02565*, 2025.
- Montúfar, G., Pascanu, R., Cho, K., and Bengio, Y. On the number of linear regions of deep neural networks. *Advances in neural information processing systems*, 27, 2014.
- Muchane, M., Richardson, S., Park, K., and Veitch, V. Incorporating hierarchical semantics in sparse autoencoder architectures. *arXiv preprint arXiv:2506.01197*, 2025.
- Munkres, J. R. *Elements of algebraic topology*. Addison-Wesley, 1984. ISBN 978-0-201-04586-4.
- Ng, A. et al. Sparse autoencoder. *CS294A Lecture notes*, 72 (2011):1–19, 2011.
- Nikolaou, G., Mencattini, T., Crisostomi, D., Santilli, A., Panagakis, Y., and Rodolà, E. Language models are injective and hence invertible. *arXiv preprint arXiv:2510.15511*, 2025.

- Oikarinen, T., Yan, G., and Weng, T.-W. Evaluating neuron explanations: A unified framework with sanity checks. *arXiv preprint arXiv:2506.05774*, 2025.
- Olah, C. Mechanistic interpretability, variables, and the importance of interpretable bases. *Transformer Circuits Thread*, 2(4), 2022.
- Olshausen, B. A. and Field, D. J. Sparse coding with an overcomplete basis set: A strategy employed by v1? *Vision research*, 37(23):3311–3325, 1997.
- Olsson, C., Elhage, N., Nanda, N., Joseph, N., DasSarma, N., Henighan, T., Mann, B., Askell, A., Bai, Y., Chen, A., et al. In-context learning and induction heads. *arXiv preprint arXiv:2209.11895*, 2022.
- O’Neill, C., Ye, C., Iyer, K., and Wu, J. F. Disentangling dense embeddings with sparse autoencoders. *arXiv preprint arXiv:2408.00657*, 2024.
- Park, K., Choe, Y. J., and Veitch, V. The linear representation hypothesis and the geometry of large language models. *arXiv preprint arXiv:2311.03658*, 2023.
- Pascanu, R., Montufar, G., and Bengio, Y. On the number of response regions of deep feed forward networks with piece-wise linear activations. *arXiv preprint arXiv:1312.6098*, 2013.
- Rajamanoharan, S., Conmy, A., Smith, L., Lieberum, T., Varma, V., Kramár, J., Shah, R., and Nanda, N. Improving dictionary learning with gated sparse autoencoders. *arXiv preprint arXiv:2404.16014*, 2024a.
- Rajamanoharan, S., Lieberum, T., Sonnerat, N., Conmy, A., Varma, V., Kramár, J., and Nanda, N. Jumping ahead: Improving reconstruction fidelity with jumprelu sparse autoencoders. *arXiv preprint arXiv:2407.14435*, 2024b.
- Ruff, L., Vandermeulen, R., Goernitz, N., Deecke, L., Siddiqui, S. A., Binder, A., Müller, E., and Kloft, M. Deep one-class classification. In Dy, J. and Krause, A. (eds.), *Proceedings of the 35th International Conference on Machine Learning*, volume 80 of *Proceedings of Machine Learning Research*, pp. 4393–4402. PMLR, 10–15 Jul 2018. URL <https://proceedings.mlr.press/v80/ruff18a.html>.
- Sarfati, R., Bigelow, E., Wurgaft, D., Merullo, J., Geiger, A., Lewis, O., McGrath, T., and Lubana, E. S. The shape of beliefs: Geometry, dynamics, and interventions along representation manifolds of language models’ posteriors. *arXiv preprint arXiv:2602.02315*, 2026.
- Shafran, O., Ronen, S., Fahn, O., Ravfogel, S., Geiger, A., and Geva, M. From directions to regions: Decomposing activations in language models via local geometry. *arXiv preprint arXiv:2602.02464*, 2026.
- Simon, E. and Zou, J. Interplm: discovering interpretable features in protein language models via sparse autoencoders. *Nature methods*, 22(10):2107–2117, 2025.
- Singh, C., Hsu, A. R., Antonello, R., Jain, S., Huth, A. G., Yu, B., and Gao, J. Explaining black box text modules in natural language with language models. *arXiv preprint arXiv:2305.09863*, 2023.
- Singh, N., Lane, S., Yu, T., Lu, J., Ramos, A., Cui, H., and Zhao, H. A generalized platform for artificial intelligence-powered autonomous enzyme engineering. *Nature communications*, 16(1):5648, 2025.
- Stanley, R. P. et al. An introduction to hyperplane arrangements. *Geometric combinatorics*, 13:389–496, 2007.
- Stokes, J. M., Yang, K., Swanson, K., Jin, W., Cubillos-Ruiz, A., Donghia, N. M., MacNair, C. R., French, S., Carfrae, L. A., Bloom-Ackermann, Z., et al. A deep learning approach to antibiotic discovery. *Cell*, 180(4): 688–702, 2020.
- Su, Y., Tang, H., Gong, Z., and Liu, Y. Sparsity is combinatorial depth: Quantifying moe expressivity via tropical geometry. *arXiv preprint arXiv:2602.03204*, 2026.
- Templeton, A. *Scaling monosemanticity: Extracting interpretable features from claude 3 sonnet*. Anthropic, 2024.
- Wang, J., Kwon, S., and Shim, B. Generalized orthogonal matching pursuit. *IEEE Transactions on signal processing*, 60(12):6202–6216, 2012.

9. Appendix

9.1. List of Contents

We organize the appendix as follows.

- **Experiment Details 9.2** describes the synthetic data generation, SAE training hyperparameters, hardware, and training time.
- **A Complete View of Concept Learning and Neuron Interpretation 9.3** includes proofs for Section 5.4.
- **Proofs for Concept Separation 9.4** contains proofs for Section 5.1.
- **Proofs for Concept Approximation 9.5** contains proofs for Section 5.2.
- **Proofs for Concept Learning Capacity 9.6** contains the proof for Section 5.3.
- **Additional Discussion on Top- K SAE 9.7** discusses the additional rank-interference effect induced by Top- K gating.

9.2. Experiment Details

For each cluster, we sample 10,000 points with uniform density. The disjoint-concept dataset contains 8 clusters, and the overlapping-concept dataset contains 12 clusters. In the overlapping dataset, the density in an overlap region is kept the same as the density in a non-overlap region. This mimics realistic concept densities: for example, the density of “red car” should not be double-counted simply because a point belongs to both “red” and “car.” We approximate the data-supported measure μ by the empirical measure on observed data. For concept approximation, we additionally sample 10,000 probe points from the blank region inside the convex hull of all observed data, i.e., $\text{Conv}(X) \setminus X$, and include these points when empirically estimating the ambient/probe measure ν .

For ReLU SAEs, we use expansion factors in $\{1, 2, 4, 8, 16, 32, 64\}$ and L_1 regularization coefficients in

$$\{10^{-5}, 5 \times 10^{-5}, 10^{-4}, 5 \times 10^{-4}, 10^{-3}, 5 \times 10^{-3}, 10^{-2}, 5 \times 10^{-2}, 10^{-1}, 5 \times 10^{-1}, 1, 3, 5, 7, 10\}.$$

For Top- K SAEs, K must not exceed the SAE width. Since the input dimension is two, the SAE width is $2EF$. We therefore use

$$K \in \{1, \dots, 2EF\} \quad \text{for } EF \in \{1, 2, 4, 8, 16\},$$

$$K \in \{1, \dots, 35, 40, 45, 50, 55, 60, 64\} \quad \text{for } EF = 32,$$

$$K \in \{1, \dots, 35, 40, 45, 50, 55, 60, 64, 80, 100, 128\} \quad \text{for } EF = 64.$$

For both architectures, we use learning rates in $\{0.1, 0.01, 0.001, 0.0003\}$ and train for 200 epochs, which is sufficient for convergence in this synthetic setting. Since our theory is constructive, we run 10 random seeds, $\{0, 1, 42, 3407, 8347, 19285, 657306, 482910, 915673, 2746089\}$, and report the best concept-learning metric across seeds. Each run is trained on one NVIDIA A40 GPU and takes approximately 5–20 minutes, depending on the expansion factor.

9.3. A Complete View of Concept Learning and Neuron Interpretation

Although neuron interpretation has not been specified in the previous sections, the theoretical results above still provide insight into it. In particular, using individual neurons or multi-neuron units for concept learning leads to different levels of interpretation quality, such as different degrees of monosemanticity. We now state the link between concept learning and neuron interpretation in an algebraic way.

Define U as the power set of all data, $U = \mathcal{P}(X)$, so that the human concept family \mathcal{C} is a finite subset of U . Define $\mathcal{N} = [d]$ as the set of neurons. Recall that $M \in \mathcal{P}(\mathcal{N})$ is a set of neurons and $\theta_M \subseteq X$ is the activation region of M . For a single neuron $N \in \mathcal{N}$, we write $\theta_N := \theta_{\{N\}}$. Since each θ_M is a subset of X , we also regard it as an element of U .

We define a binary relation $R \subseteq U \times \mathcal{N}$ by

$$CRN \iff C \subseteq \theta_N.$$

Intuitively, CRN means that neuron N is active on the whole data region C . When $C \in \mathcal{C}$, this says that N covers the whole human concept region C . This relation is not assumed to be a function: a concept may be represented by multiple neurons, and a neuron may be related to multiple concepts.

The relation R induces two maps

$$\begin{aligned} f : U &\rightarrow \mathcal{P}(\mathcal{N}), & f(C) &= \{N \in \mathcal{N} : CRN\}, \\ g : \mathcal{P}(\mathcal{N}) &\rightarrow U, & g(M) &= \bigcap_{N \in M} \theta_N, \end{aligned}$$

with the convention that $g(\emptyset) = X$. The map f sends a data region to the set of neurons that are active on the entire region. Thus, f corresponds to the concept-to-neuron direction. The map g sends a set of neurons to their common activation region. Thus, g corresponds to the neuron-to-region direction used in neuron interpretation.

Both U and $\mathcal{P}(\mathcal{N})$ are partially ordered by set inclusion. We write these posets as (U, \subseteq) and $(\mathcal{P}(\mathcal{N}), \subseteq)$. This order-

theoretic formulation is useful because it allows us to study hierarchical structure among concepts and neuron-defined regions. The larger the data region C is, the fewer neurons can be active on all of it; the larger the neuron set M is, the smaller its common activation region becomes. This is captured by the following Galois connection.

Theorem 9.1 (Galois Connection Between Human Concepts and Model Neurons). *The maps f and g form a contravariant Galois connection between U and $\mathcal{P}(\mathcal{N})$. That is, for every $C \in U$ and every $M \in \mathcal{P}(\mathcal{N})$,*

$$C \subseteq g(M) \iff M \subseteq f(C).$$

Proof. Fix $C \in U$ and $M \in \mathcal{P}(\mathcal{N})$. By the definition of g ,

$$C \subseteq g(M) \iff C \subseteq \bigcap_{N \in M} \theta_N.$$

This holds if and only if $C \subseteq \theta_N$ for every $N \in M$. By the definition of R , this is equivalent to saying that CRN for every $N \in M$. By the definition of $f(C)$, this holds if and only if every $N \in M$ belongs to $f(C)$, or equivalently $M \subseteq f(C)$. Therefore, $C \subseteq g(M) \iff M \subseteq f(C)$. \square

Intuitively, the theorem says that a data region C lies inside the common activation region of a neuron set M if and only if every neuron in M is active on the whole region C . When $C \in \mathcal{C}$, we interpret C as a human concept. The word ‘‘contravariant’’ reflects the reversal of inclusion: adding more neurons to M shrinks $g(M)$, while enlarging C can only remove neurons from $f(C)$. Therefore, the concept-learning direction f and the neuron-interpretation direction g are two sides of the same order-theoretic structure.

This Galois connection naturally induces closure operators $g \circ f$ on U and $f \circ g$ on $\mathcal{P}(\mathcal{N})$. For a data region $C \in U$, the region $g(f(C))$ is the smallest neuron-closed region, relative to the current neuron family, that contains C . If $C = g(f(C))$, then C is closed under the concept-to-neuron-to-concept operation and is called a *fixed point*. Similarly, a neuron set M is a fixed point if $M = f(g(M))$. Studying fixed points is useful for two reasons. First, different regions or neuron sets with the same closure collapse to the same canonical object, which makes redundancy visible. Second, fixed points carry lattice operations, giving a clean way to compare broader and narrower model-learned regions.

From fixed points, we define *formal concepts* as follows: a formal concept is a pair (C, M) satisfying $f(C) = M$ and $g(M) = C$. Equip formal concepts with the order

$$(C_1, M_1) \leq (C_2, M_2) \iff C_1 \subseteq C_2.$$

Equivalently, the neuron-side order is reversed: $(C_1, M_1) \leq (C_2, M_2)$ if and only if $M_2 \subseteq M_1$. The meet and join

operations are

$$\begin{aligned} (C_1, M_1) \wedge (C_2, M_2) &= (C_1 \cap C_2, f(C_1 \cap C_2)), \\ (C_1, M_1) \vee (C_2, M_2) &= (g(M_1 \cap M_2), M_1 \cap M_2). \end{aligned}$$

Intuitively, the meet gives a more specific region, $C_1 \cap C_2$, and then collects the neurons active on all of that smaller region. The join keeps the neurons shared by the two descriptions, $M_1 \cap M_2$, and returns the broader closed region described by those shared neurons. The collection of formal concepts with this order is the *concept lattice*. The U -side components C are extents, and the $\mathcal{P}(\mathcal{N})$ -side components M are intents. Extents that are not in \mathcal{C} are not necessarily meaningless; rather, they are closed regions that are not named by the chosen human concept family, and may therefore appear uninterpretable under that vocabulary.

This algebraic framework is an abstraction of the geometric framework. It gives a more general view of SAE phenomena and helps explain why concept learning can be cast as a set alignment problem between human concepts and model-learned regions.

Polysemanticity/monosemanticity. Neuron N is polysemantic when its activation region covers two unrelated concepts: there exist disjoint $C_1, C_2 \in \mathcal{C}$ with $C_1 \subseteq g(\{N\})$ and $C_2 \subseteq g(\{N\})$, i.e., the region $\theta_N = g(\{N\})$ is too coarse. If $\{N\}$ is already closed, the corresponding lattice node has extent $g(\{N\})$ and intent $\{N\}$; in general, its intent is $f(g(\{N\}))$. Its extent contains $C_1 \cup C_2$, so the current dictionary does not distinguish the two concepts inside this neuron region. Lattice operations inside this fixed context can only recombine regions already induced by the available neurons; they cannot create a new boundary inside θ_N unless some neuron already encodes that boundary. Conversely, N is monosemantic in the ideal case when $g(\{N\}) = C$ for a single $C \in \mathcal{C}$, up to the chosen notion of approximation. Disentangling a polysemantic neuron therefore requires changing the dictionary or training objective, not merely reordering one fixed lattice. This is what feature splitting attempts to do.

Feature splitting. Enlarging the SAE replaces the current neuron family Θ by a richer family Θ' . The training objective, through reconstruction under sparsity, may learn new neurons N_1, N_2, \dots with $\theta_{N_i} \approx C_i$ that did not exist in Θ . Once these neurons are present, a coarse region θ_N that previously covered several concepts can be resolved into purer regions. It is important to keep two directions separate. The actual split from coarse to fine is performed by optimization in the larger dictionary; it is what carves C_1 from C_2 . After training, the refined lattice records the result by giving the C_i their own nodes. If the old coarse feature remains, or if the refined dictionary contains shared neurons

describing it, the broad region can appear above the finer ones. Otherwise, the relation $\theta_N \approx \bigcup_i \theta_{N_i}$ should be read as an approximate geometric relation, not necessarily as an exact join inside a single intersection-based lattice.

Concept Hierarchy. This is natural in the poset. If C_{large} is more general than C_{small} , then $C_{\text{small}} \subseteq C_{\text{large}}$, and by antitonicity the neuron sets are reverse-ordered:

$$f(C_{\text{large}}) \subseteq f(C_{\text{small}}).$$

Thus, moving to a more specific concept can only add neuron constraints, while moving to a more general concept removes them. However, under a sparsity constraint, a standard SAE tends to learn a relatively flat set of features and does not explicitly represent these subconcept/superconcept containments. Capturing such hierarchy may require lattice- or graph-structured SAEs.

Feature family. A feature family can be viewed as a local part of the concept lattice around a parent concept: the nodes lying below a parent extent, or a smaller interval selected by co-activating neurons. This captures related features without forcing each member of the family to be represented by a single neuron.

Feature absorption. In the exact lattice, the hierarchy $C_{\text{small}} \subseteq C_{\text{large}}$ implies

$$f(C_{\text{large}}) \subseteq f(C_{\text{small}}).$$

That is, any neuron N that is active on the whole parent concept C_{large} must also be active on the child concept C_{small} . This gives the ideal implication

$$\begin{aligned} x \in C_{\text{small}} &\implies N \text{ activates on } x, \\ \text{for } N \in f(C_{\text{large}}). \end{aligned}$$

Feature absorption is an empirical failure of this ideal implication: a detector intended for C_{large} fails to activate on a non-negligible part of C_{small} . In the empirical relation, this means that $N \notin f(C_{\text{small}})$ even though the concept hierarchy predicts that it should be. This discrepancy suggests a simple diagnostic: list the implications $C_{\text{small}} \Rightarrow N$ predicted by the known concept hierarchy, and flag the cases where the empirical activation data do not support the implication.

9.4. Proofs for Concept Separation

Throughout this subsection, $C \in \mathcal{C}$ is a nonempty compact concept and

$$N := X \setminus C = \bigcup_{C' \in \mathcal{C}, C' \neq C} (C' \setminus C)$$

is the non-target region. We assume $|\mathcal{C}|$ is finite and $X \subset \mathbb{R}^n$ is bounded. All closures are taken in the ambient input space, and $\text{Conv}(\cdot)$ denotes convex hull.

9.4.1. PROOF OF THEOREM 5.2

We first recall two standard convexity facts.

Lemma 9.2 (Caratheodory convexity theorem (Aliprantis & Border, 2006)). *In an n -dimensional vector space, every vector in the convex hull of a nonempty set can be written as a convex combination of at most $n + 1$ points from that set.*

Corollary 9.3. (Aliprantis & Border, 2006) *The convex hull of a compact subset of a finite-dimensional vector space is compact.*

Theorem 5.2. A concept C can be separated from N with one neuron if and only if

$$\text{Conv}(C) \cap \overline{\text{Conv}(N)} = \emptyset.$$

Proof. If $N = \emptyset$, the condition is immediate and a sufficiently large bias makes any nonzero neuron positive on the bounded set C . We therefore assume $N \neq \emptyset$.

By Corollary 9.3, $K := \text{Conv}(C)$ is compact and convex. Since $N \subset X$ and X is bounded, $\text{Conv}(N)$ is bounded; hence $L := \overline{\text{Conv}(N)}$ is compact by the Heine–Borel theorem (Munkres, 1984). The set L is also convex because the closure of a convex set is convex.

Recall that separation by one neuron means that there are $w \in \mathbb{R}^n \setminus \{0\}$ and $b \in \mathbb{R}$ such that

$$w^\top x + b > 0 \quad (x \in C), \quad w^\top y + b \leq 0 \quad (y \in N). \quad (7)$$

Equivalently, with $\beta := -b$, we require $w^\top x > \beta$ on C and $w^\top y \leq \beta$ on N . The usual hyperplane-separation theorem almost gives this result, but here the positive side is strict while the negative side is weak. We therefore give the direct proof.

(\Leftarrow) Assume $K \cap L = \emptyset$. Since K and L are nonempty compact sets, the continuous map $(u, v) \mapsto \|u - v\|$ attains its minimum over $K \times L$ at some (u^*, v^*) . Let

$$\delta := \|u^* - v^*\|, \quad w := u^* - v^*.$$

Because $K \cap L = \emptyset$, we have $\delta > 0$ and $w \neq 0$.

For any $u \in K$ and $t \in [0, 1]$, convexity gives $u^* + t(u - u^*) \in K$. By minimality,

$$\|u^* + t(u - u^*) - v^*\|^2 \geq \|u^* - v^*\|^2.$$

Expanding, dividing by $t > 0$, and sending $t \rightarrow 0^+$ gives

$$w^\top u \geq w^\top u^* \quad (u \in K). \quad (8)$$

Similarly, varying $v \in L$ while keeping u^* fixed yields

$$w^\top v \leq w^\top v^* \quad (v \in L). \quad (9)$$

Moreover,

$$w^\top u^* - w^\top v^* = w^\top (u^* - v^*) = \|w\|^2 = \delta^2 > 0. \quad (10)$$

Set $\beta := \frac{1}{2}(w^\top u^* + w^\top v^*)$ and $b := -\beta$. For $x \in C \subseteq K$, equations (8) and (10) imply

$$w^\top x + b \geq w^\top u^* - \beta = \frac{1}{2}\delta^2 > 0.$$

For $y \in N \subseteq \text{Conv}(N) \subseteq L$, equations (9) and (10) imply

$$w^\top y + b \leq w^\top v^* - \beta = -\frac{1}{2}\delta^2 < 0.$$

Thus (w, b) satisfies (7).

(\Rightarrow) Conversely, suppose (w, b) satisfies (7), and set $\beta := -b$. Then $w^\top x > \beta$ for all $x \in C$ and $w^\top y \leq \beta$ for all $y \in N$.

By Lemma 9.2, each $u \in \text{Conv}(C)$ is a finite convex combination $u = \sum_j \lambda_j x_j$ with $x_j \in C$, $\lambda_j \geq 0$, and $\sum_j \lambda_j = 1$. Therefore

$$w^\top u = \sum_j \lambda_j w^\top x_j \geq \min_j w^\top x_j > \beta,$$

where the final strict inequality is valid because the minimum is over finitely many terms. Hence

$$w^\top u > \beta \quad (u \in \text{Conv}(C)). \quad (11)$$

The same finite-convex-combination argument gives $w^\top v \leq \beta$ for all $v \in \text{Conv}(N)$. By continuity, this extends to

$$w^\top v \leq \beta \quad (v \in \overline{\text{Conv}(N)}). \quad (12)$$

If a point p belonged to both $\text{Conv}(C)$ and $\overline{\text{Conv}(N)}$, equations (11) and (12) would give the contradiction $w^\top p > \beta$ and $w^\top p \leq \beta$. Thus the two sets are disjoint. \square

In infinite-dimensional settings, such as an RKHS induced by an RBF kernel, the convex hull of a compact concept need not be compact without additional assumptions. In that case, the natural replacement is the closed convex hull, denoted $\overline{\text{Conv}(C)}$. In complete metrizable locally convex spaces, the closed convex hull of a compact set is compact (Aliprantis & Border, 2006). Since the closure of a convex set is convex, this closed convex hull is exactly the closure of the ordinary convex hull.

9.4.2. PROOF OF COROLLARY 5.3

Corollary 5.3.

1. All concepts in \mathcal{C} can be separated from each other by one neuron per concept if and only if

$$\text{Conv}(C_i) \cap \overline{\text{Conv}(N_i)} = \phi \quad (C_i \in \mathcal{C}),$$

where $N_i = X \setminus C_i$.

2. If perfect one-neuron separation is possible for all distinct, nonempty concepts in a finite \mathcal{C} , then at least $|\mathcal{C}|$ neurons are necessary and $|\mathcal{C}|$ neurons are sufficient.

Proof. The first claim follows by applying Theorem 5.2 to each concept C_i with $N_i = X \setminus C_i$.

For the second claim, sufficiency follows from the first claim: each concept can be assigned one separating neuron. For necessity, suppose a neuron with activation region H^+ perfectly represents two concepts C_i and C_j . Perfect separation gives $H^+ \cap X = C_i$ and also $H^+ \cap X = C_j$, so $C_i = C_j$. Thus distinct concepts cannot share the same one-neuron representation, and at least $|\mathcal{C}|$ neurons are required. \square

9.4.3. PROOF OF THEOREM 5.4

We first record a strict point-versus-convex-set separation lemma.

Lemma 9.4 (Strict separation of a point). *Let $K \subseteq \mathbb{R}^n$ be nonempty, compact, and convex, and let $y \notin K$. Then there exist $w \neq 0$ and $\beta \in \mathbb{R}$ such that*

$$w^\top y < \beta, \quad w^\top u > \beta \quad (u \in K).$$

Proof. Since K is compact, the map $u \mapsto \|u - y\|$ attains its minimum at some $u^* \in K$. Because $y \notin K$, $\delta := \|u^* - y\| > 0$. Let $w := u^* - y$. For $u \in K$ and $t \in [0, 1]$, convexity gives $u^* + t(u - u^*) \in K$, and minimality gives

$$\|u^* + t(u - u^*) - y\|^2 \geq \|u^* - y\|^2.$$

Expanding and letting $t \rightarrow 0^+$ yields $w^\top (u - u^*) \geq 0$, so

$$w^\top u \geq w^\top u^* = w^\top y + \|w\|^2 \quad (u \in K).$$

Choosing $\beta := w^\top y + \frac{1}{2}\|w\|^2$ proves the claim. \square

Theorem 5.4. A concept C can be separated from N by a unit if and only if

$$\text{Conv}(C) \cap \overline{N} = \phi.$$

Proof. A unit is a finite intersection of neuron activation regions. Given neurons $(w_i, b_i)_{i=1}^m$, write

$$\theta := \bigcap_{i=1}^m \{x : w_i^\top x + b_i > 0\}.$$

Separating C from N by this unit means

$$C \subseteq \theta, \quad N \cap \theta = \phi, \quad (13)$$

or equivalently, every point in C activates all selected neurons, while every point in N fails to activate at least one selected neuron.

(\Leftarrow) Assume $\text{Conv}(C) \cap \overline{N} = \phi$. Let $K := \text{Conv}(C)$, which is nonempty, compact, and convex by Corollary 9.3. The set \overline{N} is compact because $N \subseteq X$ and X is bounded.

For each $y \in \overline{N}$, Lemma 9.4 gives $w_y \neq 0$ and β_y such that

$$w_y^\top y < \beta_y, \quad w_y^\top u > \beta_y \quad (u \in K). \quad (14)$$

The open halfspaces $U_y := \{x : w_y^\top x < \beta_y\}$ form an open cover of \overline{N} . By compactness, choose a finite subcover U_{y_1}, \dots, U_{y_m} . Define neurons by $(w_i, b_i) := (w_{y_i}, -\beta_{y_i})$ and set

$$\theta = \bigcap_{i=1}^m \{x : w_i^\top x + b_i > 0\}.$$

For every $x \in C \subseteq K$, the second inequality in (14) gives $w_i^\top x + b_i > 0$ for all i , so $C \subseteq \theta$. For every $y \in N \subseteq \overline{N}$, the finite subcover gives some i with $y \in U_{y_i}$, hence $w_i^\top y + b_i < 0$ and $y \notin \theta$. Therefore $N \cap \theta = \phi$.

(\Rightarrow) Conversely, suppose a finite unit θ satisfies (13). We first show that $\text{Conv}(C) \subseteq \theta$. For any $u \in \text{Conv}(C)$, write $u = \sum_j \lambda_j x_j$ with $x_j \in C$, $\lambda_j \geq 0$, and $\sum_j \lambda_j = 1$. For each selected neuron i ,

$$w_i^\top u + b_i = \sum_j \lambda_j (w_i^\top x_j + b_i) > 0,$$

because each term is positive. Hence $u \in \theta$.

If $p \in \text{Conv}(C) \cap \overline{N}$, then $p \in \theta$. Since θ is open and $p \in \overline{N}$, there exists a sequence $y_k \in N$ with $y_k \rightarrow p$ and eventually $y_k \in \theta$, contradicting $N \cap \theta = \phi$. Thus $\text{Conv}(C) \cap \overline{N} = \phi$. \square

9.4.4. PROOF OF COROLLARY 5.5

Corollary 5.5. Assume \mathcal{C} is finite. All concepts in \mathcal{C} can be separated from each other by units if and only if

$$\text{Conv}(C_i) \cap \overline{(C_j \setminus C_i)} = \phi \quad (C_i, C_j \in \mathcal{C}, C_j \neq C_i).$$

Proof. Fix $C_i \in \mathcal{C}$ and write

$$N_i := X \setminus C_i = \bigcup_{j \neq i} (C_j \setminus C_i).$$

By Theorem 5.4, C_i can be separated from N_i by a unit if and only if

$$\text{Conv}(C_i) \cap \overline{N_i} = \phi.$$

Since \mathcal{C} is finite,

$$\overline{N_i} = \overline{\bigcup_{j \neq i} (C_j \setminus C_i)} = \bigcup_{j \neq i} \overline{(C_j \setminus C_i)}.$$

Therefore

$$\begin{aligned} \text{Conv}(C_i) \cap \overline{N_i} = \phi \\ \iff \\ \text{Conv}(C_i) \cap \overline{(C_j \setminus C_i)} = \phi \quad \text{for all } j \neq i. \end{aligned}$$

Taking the conjunction over all i proves the equivalence. \square

Neuron-budget remark. The equivalence above guarantees that each concept can be separated by some finite unit, but the number of halfspaces obtained from the compact-cover proof depends on the geometry of the sets. A geometry-independent bound of $|\mathcal{C}|(|\mathcal{C}|-1)$ neurons follows under the stronger pairwise one-neuron condition

$$\text{Conv}(C_i) \cap \overline{\text{Conv}(C_j \setminus C_i)} = \phi \quad (i \neq j).$$

Indeed, Theorem 5.2 then gives one neuron that is positive on C_i and non-positive on $C_j \setminus C_i$ for each ordered pair (i, j) . Intersecting the $|\mathcal{C}| - 1$ neurons associated with a fixed i separates C_i from $X \setminus C_i$. Across all concepts this uses at most $|\mathcal{C}|(|\mathcal{C}| - 1)$ neurons before any reuse. Under the weaker condition of Corollary 5.5, the correct general statement is finiteness, not a universal $|\mathcal{C}|(|\mathcal{C}| - 1)$ bound.

This explains why units can be more monosemantic than individual neurons: neurons can be reused across several units, and each unit can combine several halfspaces to exclude different non-target regions.

9.4.5. DISCUSSION OF DEFINITION 5.6

Recall that the separation error is the symmetric difference on the data support:

$$e_{\text{sep}}(C, \theta) = \mu(C \Delta \theta) = \underbrace{\mu(\theta \setminus C)}_{\text{contamination error } e_c} + \underbrace{\mu(C \setminus \theta)}_{\text{missing error } e_m},$$

where μ is a Borel probability measure supported on X .

An equivalent form is

$$e_{\text{sep}}(C, \theta) = \mu(C \setminus \theta) + \mu\left(\theta \cap \bigcup_{C' \in \mathcal{C}, C' \neq C} (C' \setminus C)\right).$$

The second term measures how much unrelated concept mass is covered by θ .

Proof. Because $X = \bigcup_{C' \in \mathcal{C}} C'$, we have

$$\bigcup_{C' \in \mathcal{C}, C' \neq C} (C' \setminus C) = X \setminus C.$$

For concept separation, $\theta \subseteq X$, and hence

$$\theta \cap \bigcup_{C' \in \mathcal{C}, C' \neq C} (C' \setminus C) = \theta \cap (X \setminus C) = \theta \setminus C.$$

Finally,

$$C \Delta \theta = (C \setminus \theta) \cup (\theta \setminus C),$$

where the union is disjoint. Additivity of μ gives the claimed expression. \square

9.5. Proofs for Concept Approximation

For the approximation results, we work on a bounded convex probe domain $\Omega \subset \mathbb{R}^n$ containing the support on which the approximation error is evaluated. We assume that ν has a density with respect to the relevant Lebesgue measure on Ω , bounded above and below on its support. These regularity assumptions rule out purely atomic or otherwise degenerate probe measures, for which arbitrary labels on finitely many atoms may not reflect the ambient geometry.

9.5.1. PROOF OF THEOREM 5.8

Theorem 5.8. A concept $C \in \mathcal{C}$ can be arbitrarily well approximated under the approximation error by units if and only if C is convex up to a ν -null set.

Proof. Here ‘‘convex up to a ν -null set’’ means that there exists a convex set K such that $\nu(C\Delta K) = 0$.

(\Leftarrow) Suppose such a convex set K exists. Standard convex-body approximation gives a sequence of polytopes P_m , each representable as an intersection of finitely many halfspaces, such that $\nu(K\Delta P_m) \rightarrow 0$. Each P_m can be implemented by a unit, up to boundary sets of ν -measure zero. Therefore

$$\nu(C\Delta P_m) \leq \nu(C\Delta K) + \nu(K\Delta P_m) \rightarrow 0,$$

so C can be arbitrarily well approximated by units.

(\Rightarrow) Conversely, suppose there exist units θ_m such that $\nu(C\Delta\theta_m) \rightarrow 0$. Each θ_m is convex because it is an intersection of halfspaces. Intersecting with the bounded domain $\text{Supp}(\nu)$ and taking closures changes the sets only on polyhedral boundaries, which are ν -null; thus, the compact convex sets $K_m := \overline{\theta_m \cap \text{Supp}(\nu)}$ still satisfy $\nu(C\Delta K_m) \rightarrow 0$. By the compactness theorem for convex bodies on a bounded domain, a subsequence of K_m converges in Hausdorff distance to a compact convex set $K \subseteq \text{Supp}(\nu)$. Since Hausdorff convergence of convex bodies implies convergence in measure, $\nu(K_m\Delta K) \rightarrow 0$ along this subsequence. Therefore

$$\nu(C\Delta K) \leq \nu(C\Delta K_m) + \nu(K_m\Delta K) \rightarrow 0,$$

so $\nu(C\Delta K) = 0$. Thus C is convex up to a ν -null set. \square

9.5.2. PROOF OF THEOREM 5.9

Theorem 5.9. Under regularity and boundary-smoothness conditions, a concept $C \in \mathcal{C}$ can be approximated by a unit θ_M with error

$$e_{\text{app}}(C, \theta_M) \lesssim e_{\text{irr}} + A|M|^{-\frac{2}{r-1}},$$

where A depends on boundary smoothness, r is the effective dimension of C , and e_{irr} is an irreducible convexification error. In particular, $e_{\text{irr}} = 0$ when C is convex, or more generally when $\nu(\text{Conv}(C) \setminus C) = 0$.

Proof. We first consider the convex case. Let $m := |M|$. Assume that C is an r -dimensional convex body, $r \geq 2$, with \mathcal{C}^2 boundary and positive Gaussian curvature, and that ν has positive continuous density ρ_ν with respect to r -dimensional Lebesgue measure on the affine hull of C . The case $r = 1$ is simpler: an interval can be represented exactly by two halfspaces, up to boundary measure zero.

A unit with m selected neurons is an intersection of m halfspaces, hence a polytope with at most m facets. Conversely, any such polytope can be represented by a unit with at most m neurons. Theorem 3 of Ludwig (1999) gives the asymptotic best approximation rate by m -facet polytopes:

$$\inf_{\theta_M: |M|=m} \nu(C\Delta\theta_M) \sim \frac{1}{2} \text{ldiv}_{r-1} \left(\int_{\partial C} \rho_\nu(x)^{\frac{r-1}{r+1}} \kappa_C(x)^{\frac{1}{r+1}} d\mathcal{H}^{r-1}(x) \right)^{\frac{r+1}{r-1}} m^{-\frac{2}{r-1}}.$$

Absorbing the boundary integral and dimension-dependent constants into A yields

$$e_{\text{app}}(C, \theta_M) \lesssim Am^{-\frac{2}{r-1}}.$$

For a non-convex concept, let K be a convex body used as a convex envelope for C ; when $\text{Conv}(C)$ satisfies the same regularity assumptions, we may take $K = \text{Conv}(C)$. Let θ_M be the m -facet unit approximating K . By the triangle inequality for symmetric difference,

$$\nu(C\Delta\theta_M) \leq \nu(C\Delta K) + \nu(K\Delta\theta_M) \lesssim \nu(C\Delta K) + A_K m^{-\frac{2}{r-1}}.$$

The first term is the irreducible error caused by approximating a non-convex set with convex units. Taking $K = \text{Conv}(C)$ gives $e_{\text{irr}} = \nu(\text{Conv}(C) \setminus C)$ whenever $C \subseteq \text{Conv}(C)$ is evaluated under ν ; more generally, e_{irr} may be defined as the best such convex-envelope error over admissible convex K . This proves the claimed upper bound. \square

9.6. Proofs for Concept Learning Capacity

Theorem 5.10. Suppose perfect monosemanticity holds for all concepts, and each concept is represented by at most k_c neurons. In the regime $d \gg k_c$, this requires approximately

$$d \gtrsim (k_c! |\mathcal{C}|)^{1/k_c},$$

where d is the number of non-dead neurons.

Proof. If each concept is represented by at most k_c neurons, then the number of possible nonempty neuron sets is

$$\sum_{r=1}^{k_c} \binom{d}{r}.$$

Perfect monosemanticity requires the concept-to-unit map $f : \mathcal{C} \rightarrow \Theta$ to be injective, so two distinct concepts cannot be assigned to the same neuron set. Therefore

$$|\mathcal{C}| \leq \sum_{r=1}^{k_c} \binom{d}{r}.$$

When $d \gg k_c$, the leading term is

$$\binom{d}{k_c} = \frac{d^{k_c}}{k_c!} (1 + o(1)).$$

Thus a necessary asymptotic scaling is

$$\frac{d^{k_c}}{k_c!} \gtrsim |\mathcal{C}|,$$

which gives

$$d \gtrsim (k_c! |\mathcal{C}|)^{1/k_c}.$$

□

9.7. Additional Discussion on Top- K SAE

For Top- K SAE, write $z_i(x) = \langle w_i, x \rangle + b_i$. The SNTA of neuron i is

$$N_i^{\text{topk}} = \{x \in X : z_i(x) > \tau_i \text{ and } i \in \text{TopK}_k(z(x))\}.$$

Thus $N_i^{\text{topk}} \subseteq H_i^+$. For a set of neurons M ,

$$\theta_M^{\text{topk}} = \bigcap_{j \in M} N_j^{\text{topk}}.$$

If $|M| > k$, then $\theta_M^{\text{topk}} = \phi$. If $|M| \leq k$, then θ_M^{topk} equals the absolute-gating region $\bigcap_{j \in M} H_j^+$ after removing points where at least one neuron in M fails to enter the top- k set. This is the relative-gating effect.

Let

$$P_M := \bigcap_{j \in M} H_j^+, \quad Q_M := \theta_M^{\text{topk}}.$$

Then $Q_M \subseteq P_M$. Define the rank-interference region

$$I_M := P_M \setminus Q_M.$$

For any concept C and any measure η equal to either μ or ν ,

$$\eta(C \Delta Q_M) = \eta(C \Delta P_M) + \eta(C \cap I_M) - \eta((P_M \setminus C) \cap I_M).$$

Indeed, $Q_M = P_M \setminus I_M$, so replacing P_M by Q_M adds false negatives on $C \cap I_M$ and removes false positives on $(P_M \setminus C) \cap I_M$.

Therefore, Top- K gating can hurt by removing true target points, but it can also help by removing false positives outside the target. The absolute-gating results transfer cleanly to Top- K only when the rank-interference term is small on the target concept, or when its false-positive reduction outweighs the additional false negatives.